NAVAL POSTGRADUATE SCHOOL

MONTEREY, CALIFORNIA

THESIS

TAIL SEPARATION AND DENSITY EFFECTS ON THE UNDERWATER TRAJECTORY OF THE JDAM

by

Jillene Marie Bushnell

December 2009

Thesis Advisor:	Peter Chu
Second Reader:	Brian Almquist

Approved for public release; distribution is unlimited

REPORT DOCUMENTATION PAGE		Form Approved OMB No. 0704-0188

1. AGENCY USE ONLY *(Leave blank)*	2. REPORT DATE December 2009	3. REPORT TYPE AND DATES COVERED Master's Thesis

4. TITLE AND SUBTITLE Tail Separation and Density Effects on the Underwater Trajectory of the JDAM	5. FUNDING NUMBERS
6. AUTHOR(S) Bushnell, Jillene M.	
7. PERFORMING ORGANIZATION NAME(S) AND ADDRESS(ES) Naval Postgraduate School Monterey, CA 93943-5000	**8. PERFORMING ORGANIZATION REPORT NUMBER**
9. SPONSORING /MONITORING AGENCY NAME(S) AND ADDRESS(ES) NAVOCEANO, Stennis Space Center, MS 39522-5001 Institute of Joint Warfare Analysis, NPS, Monterey, CA, 93943	**10. SPONSORING/MONITORING AGENCY REPORT NUMBER**

11. SUPPLEMENTARY NOTES The views expressed in this thesis are those of the author and do not reflect the official policy or position of the Department of Defense or the U.S. Government.

12a. DISTRIBUTION / AVAILABILITY STATEMENT Approved for public release, distribution is unlimited	12b. DISTRIBUTION CODE

13. ABSTRACT (maximum 200 words)

The Navy is in need of an organic, inexpensive, swift method to neutralize or sweep waterborne mines. This thesis presents an alternative to current mine countermeasure technologies that fulfills this criteria—the use of the Joint Direct Attack Munition (JDAM) to clear a minefield. It updates the general, physics-based, six degrees of freedom model, STRIKE35, to predict the three-dimensional, free-fall trajectory and orientation of a MK-84 bomb (simulating the JDAM) through a water column. It accurately predicts the final detonation position relative to an underwater mine in the very shallow water environment. Input parameters include accurate water impact speed and surface impact angle of attack. Because the model results compare well with experimental data from the Stand-Off Assault Breaching Weapon Fuze Improvement (SOABWFI) Program, we analyzed the trajectory of the weapon with structural failures. This thesis solves for the impact speed and impact angle of attack limitations to remain within the Technology Transition Agreement, the detonation location for each fuze delay setting (to include its 20% tolerance), and the trajectory changes due to different water densities. This gives strike planners a tactical decision aid to clear the minefield accurately and efficiently with existing aircraft and weapons.

14. SUBJECT TERMS Hydrodynamic, STRIKE35, Joint Direct Attack Munition (JDAM), Mine Countermeasure (MCM), Mine, Improvised Explosive Device (IED), Numerical Modeling, Stand-off Assault Breaching Weapon Fuze Improvement (SOABWFI)	15. NUMBER OF PAGES 104
	16. PRICE CODE

17. SECURITY CLASSIFICATION OF REPORT	18. SECURITY CLASSIFICATION OF THIS PAGE	19. SECURITY CLASSIFICATION OF ABSTRACT	20. LIMITATION OF ABSTRACT
Unclassified	Unclassified	Unclassified	UU

NSN 7540-01-280-5500

Standard Form 298 (Rev. 2-89)
Prescribed by ANSI Std. 239-18

THIS PAGE INTENTIONALLY LEFT BLANK

Approved for public release; distribution is unlimited

TAIL SEPARATION AND DENSITY EFFECTS ON THE UNDERWATER TRAJECTORY OF THE JDAM

Jillene M. Bushnell
Lieutenant Commander, United States Navy
B.S., United States Naval Academy, 1998

Submitted in partial fulfillment of the
requirements for the degree of

**MASTER OF SCIENCE IN
METEOROLOGY AND PHYSICAL OCEANOGRAPHY**

from the

**NAVAL POSTGRADUATE SCHOOL
December 2009**

Author: Jillene Marie Bushnell, LCDR USN

Approved by: Peter Chu
Thesis Advisor

Brian Almquist
Second Reader

Jeffrey Paduan
Chairman, Department of Oceanography

THIS PAGE INTENTIONALLY LEFT BLANK

ABSTRACT

The Navy is in need of an organic, inexpensive, swift method to neutralize or sweep waterborne mines. This thesis presents an alternative to current mine countermeasure technologies that fulfills this criteria—the use of the Joint Direct Attack Munition (JDAM) to clear a minefield. It updates the general, physics-based, six degrees of freedom model, STRIKE35, to predict the three-dimensional, free-fall trajectory and orientation of a MK-84 bomb (simulating the JDAM) through a water column. It accurately predicts the final detonation position relative to an underwater mine in the very shallow water environment. Input parameters include accurate water impact speed and surface impact angle of attack. Because the model results compare well with experimental data from the Stand-Off Assault Breaching Weapon Fuze Improvement (SOABWFI) Program, we analyzed the trajectory of the weapon with structural failures. This thesis solves for the impact speed and impact angle of attack limitations to remain within the Technology Transition Agreement, the detonation location for each fuze delay setting (to include its 20% tolerance), and the trajectory changes due to different water densities. This gives strike planners a tactical decision aid to clear the minefield accurately and efficiently with existing aircraft and weapons.

THIS PAGE INTENTIONALLY LEFT BLANK

TABLE OF CONTENTS

LIST OF FIGURES

LIST OF TABLES

THIS PAGE INTENTIONALLY LEFT BLANK

ACKNOWLEDGMENTS

My sincerest gratitude goes out to. . .

- Professor Peter Chu and Mr. Chenwu Fan, for their assistance and expertise throughout my analysis.

- Mr. Brian Almquist, for the ability to participate in SOABWFI, as well as expert guidance.

- Mr. Kennard Watson, for the ability to participate in SOABWFI, as well as editing and improving this thesis tremendously.

- Kris, my husband who stayed up many nights while I worked, for the love and support you are forever giving to me.

- My sons, Noah and Mitchell, for the happiest days I've ever known.

THIS PAGE INTENTIONALLY LEFT BLANK

I. INTRODUCTION

A. ECONOMY AND SECURITY

The global economy in which we prosper is due solely to the free movement of goods and services secured by the world's navies, most specifically, our own. The oceans support 90% of the world's trade and two-thirds of its petroleum transport. In the joint doctrine, *A Cooperative Strategy for 21st Century Seapower*, the heads of the U.S. maritime forces accurately describe the sea-lanes and supporting shore infrastructure as "lifelines of the modern global economy, visible and vulnerable symbols of the modern distribution system that relies on free transit through increasingly urbanized littoral regions" (Conway et al. 2007).

Even shutting down a single port can have devastating consequences on a nation's economy. During RADM Hine's 2005 brief to the Mine Warfare Association, he told of the ripple effect that closing Long Beach port caused to other sectors of the U.S. economy in the fall of 2002. He described the ten-day lockout as taking three and a half months to clear the container backlog, even after they took mitigating measures in anticipation of the strike. He also showed a table, which he said was "dated." Table 1 presents the value of cargo handled by the top ten U. S. ports, showing the enormity of economic damage a port closure would cause. In fact, the widely quoted estimate claims a shutdown of port facilities would cost the U.S. economy $1.94 billion per day (Hall 2004).

Port	$Million/day
Los Angeles	278.9
Long Beach	269.0
New York	221.6
Houston	118.9
Seattle	88.5
Charleston	86.3
Hampton Roads	77.8
Oakland	68.5
Baltimore	56.4
Tacoma	53.4

Table 1. Top ten U. S. ports by value of cargo handled [From Hines 2005]

While the previous examples of financial impact are specific to the U.S., they serve to illustrate the overall criticality of the flow of international commerce, including energy supplies. There is also no denying the inextricable link between a country's prosperity and its security. To protect and sustain global stability and interdependent networks, we need to maintain control of the sea. Nevertheless, laying mines is a relatively simple method to interrupt or deny this control. However, ports and chokepoints are not the only places vulnerable to disruption. During operations other than peace, sea-lines of communication and beaches for amphibious landings are also easy targets for mining.

B. THE THREAT

Mines are prolific. Currently, there are over 50 countries possessing the capability to mine. Of these, at least 30 have demonstrated production capability and 20 have attempted to export. Commercialization and foreign military sales programs currently drive the abundance of mines (Federation of American Scientists 2008). Because mines are a flexible and relatively simple means of denying the use of an area, they are the perfect "fire and forget" weapon.

One cannot ignore a mine threat. No matter if mining is only threatened or actual mining takes place the same action occurs to meet the potential threat. Calculating the value of a minefield, one can sum up the amount of time an area was denied, the man-

hours invested to open the area for transit, the number of ships hit or needing repair, and the number of people injured or killed. As long as the effect outweighs the cost, the tactic is effective. Considering the production and mine-laying cost is less than 10% that of removal, and it taking hundreds of times longer, mines are a very effective weapon (Brown 1991 and Naval Studies Board National Research Council 2001).

When a mine explodes near a ship, the effects can be devastating and the repair costs exorbitant. In the past 60 years, 79% of the 19 U. S. Navy ships that have suffered battle damage were the result of waterborne mines (Bruhn 2006). Of these, only one was from a modern, more expensive mine (Naval War College 2009a). This means they are also attractive weapons for asymmetric warfare since they are relatively low cost - as little as a few hundred U.S. dollars for a simple contact mine (Zolton 1991). Figure 1 shows the return on investment for mines in the Gulf War. Moored mines (left, grey) are so inexpensive that even an individual could buy them. Even the more expensive bottom mine (right, blue) is only a fraction of the repair price.

Figure 1. Mines: favorable investment return [From Naval War College 2009a]

C. TODAY'S DEFENSE

1. Getting on Station

The cost of repairing ships does not solely drive this problem. The price of getting the correct equipment to and neutralizing the minefield can cost as much or more than the repair. Currently Mine Countermeasure ships (SMCM) are in San Diego, Sasebo, and Manama while the Mine Countermeasure aircraft (AMCM) are in Norfolk and Manama (Figure 2). Though these forward deployed locations are in the correct place strategically, limited assets obviously cannot be at every chokepoint or super port in the world. Since both surface and air mine countermeasures (MCMs) are slow moving and are near the end of their service life, they typically get transported via air or sea if an emergency occurs away from their current operating area.

Figure 2. Chokepoints and super ports [After Naval War College 2009a]

Military airlift is the fastest mode of transportation, but it is also the most expensive. The typical airframe cost per flight hour is about $5,000 for the C-17, about $6,000 for the C-5, and about $1,500 for the C-130 (Federation of American Scientists

2009). This assumes that the aircraft can land close enough to the area denied by mines. In order to accomplish this, we must have air superiority prior to flying an undefended aircraft into the area. It also means the airfield is large and strong enough for the aircraft to land, there is room for the offload of the MCMs, and transportation is available to get the SMCM to the water (Naval War College 2009c).

The Military Sealift Command (MSC) has the quickest cargo ships in the world, the Fast Sealift Ships (T-AKR). They are for rapid deployment of equipment around the world and are normally in a reduced operating status with the ability to get underway to load ports within 96 hours (Military Sealift Command 2003). Their transit speed is up to 24 kts, which means it will take about 18 days to make the 8,600 nm trip from Norfolk to the Persian Gulf. Still, this method can preserve service life and reduce transit time by up to 50% (USS Ardent).

2. Once on Station

In order for the MCMs to work an area, there must not be a threat else they need protection. They lack the ability to defend themselves, except for close in armaments: machine guns (A/SMCM) and grenade launcher (SMCM). If threatened by an adversary, MCMs are unable to continue their work as they are restricted in their maneuvering. Though AMCMs are able to sweep for mines faster than their surface counterparts, what they gain in speed, they give up in effectiveness and stamina. AMCMs also require flight time from their base (whether a ship or an airport). Nonetheless, they are more capable in the shallow water to very shallow water (VSW) environments (Figure 3) due to the 25-foot navigational draft restrictions of the SMCM.

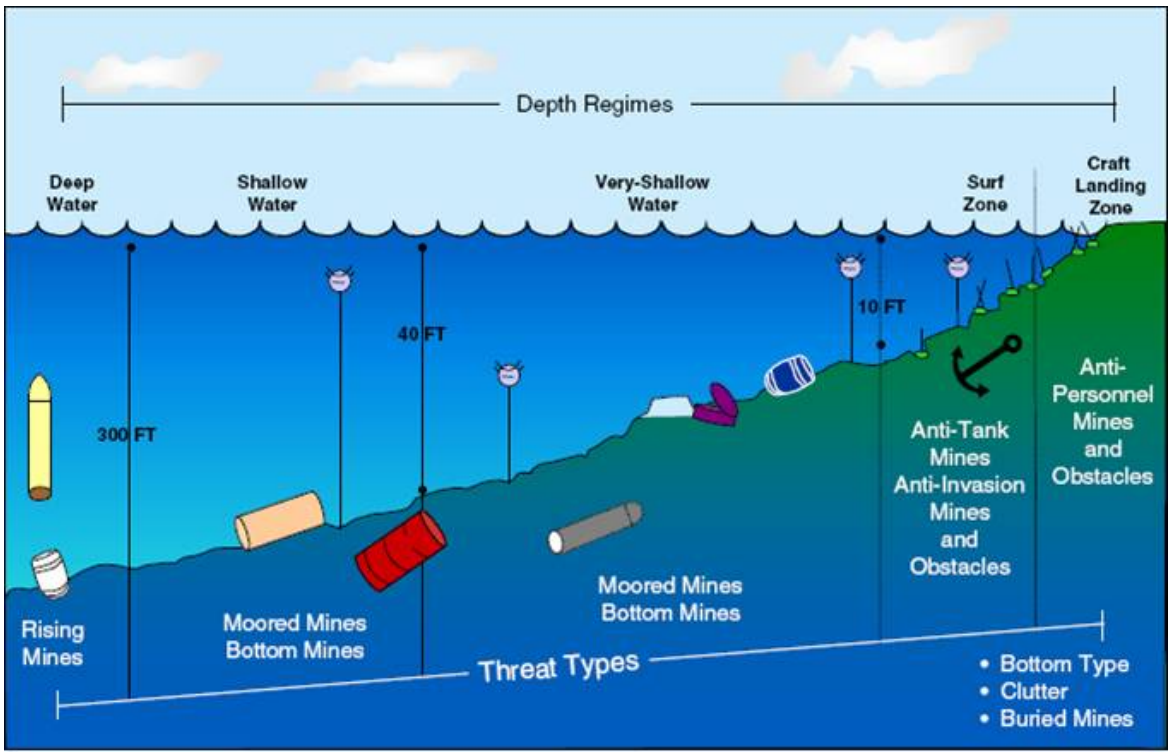

Figure 3. Undersea battlespace and types of mines found in each depth [From United States General Accounting Office 2001]

SMCMs sweep very effectively in a straight line, at depths greater than 25 feet, at about 8-10 knots. The size of the area then determines how long the sweep will take. They are also able to hunt for mine-like-objects, and then send an Explosive Ordinance Disposal (EOD) technician or the AN/SLQ-48 Mine Neutralization Vehicle (MNV) to inspect or destroy the object (Gasperini 2003). This shows that time is the biggest factor in how well an area can be cleared. The measure of success is then a probability, e.g. a 95% confidence that the area has a 67% clearance rating. There is always a balance between time and risk, so a constrained timeline causes the acceptance of more risk.

Many options exist to neutralize mines, but all options have advantages as well as disadvantages. For example, SMCMs are extremely effective but are slow and have draft limitations that do not allow them to operate in shallow water. SMCMs have the AN/SLQ-48 Mine Neutralization System (an autonomous submersible for moored and bottom mines), but these are also slow. AMCMs can tow the very capable sled (with the

MK-103 through MK-106 installed) into shallow water, but are unable to work in low visibility or at night. EOD technicians are excellent in the VSW, but their limitations come from fatigue, water temperatures, and water depth. Beyond the risk they are taking being in the water, if the water is murky enough to restrict vision, their risk increases. Marine mammals, though excellent at hunting mines and currently our only asset for detection of buried mines, do not neutralize mines due to the risk involved with handling explosives (Bruhn 2007 and Naval Studies Board National Research Council 2001). In order to reduce the risk to personnel and to reduce the sweep timeline without sacrificing effectiveness, a balance of assets is currently the best available option (Naval War College 2009a).

D. TOMORROW'S DEFENSE

In order to further decrease MCM response time and increase MCM capabilities, the Navy is currently integrating MCM forces, both physically and doctrinally, into all Navy Joint Task Forces. This reduces the reliance on dedicated MCM forces in the early stages of a conflict (Mullen 2000). Future dedicated capabilities include the Littoral Combat Ship (LCS) to replace the Avenger class (SMCM) and the MH-60S Knighthawk to replace the MH-53E Sea Dragon (AMCM), just to name a few (Hines 2005). These systems, among others, had an initial forecast completion of FY10, but according to RADM Hines (2005), the "initial program introductions continue to slip to the right."

The future of mine warfare (MIW) is at the mercy of technology. What happens to our fleet of SMCM and AMCM if an "unsweepable" mine is developed? Currently, modern mines have delayed arming devices, ship counters, clock-controlled live periods, and the ability to classify mine-hunting ships (Hartmann and Truver 1991). This paper proposes adding an off-the-shelf asset to the mix of current mine neutralizers that is not effected by the limitations of the "unsweepable" mine. The capability of the Joint Direct Attack Munition (JDAM) Assault Breaching System (JABS), readily available in any Strike Group, is an essential addition to the MCM solution.

THIS PAGE INTENTIONALLY LEFT BLANK

II. RESEARCH OBJECTIVE

A. PREVIOUS

> Because of a lack of immediately available mine counter measures in any large quantities, the Navy is evaluating the JDAM Assault Breaching System (JABS) for its capability in countermine and assault breaching. The JDAM accuracy, repeatability (guaranteed delivery patterns for multiple deliveries) and fuzing options make the JABS a prime contender for an interim capability. Combined with bomber range and payload capability, this weapon system vastly improves joint operations. (Almquist 2008)

To bridge the gap between developing and aging systems, the Office of Naval Research (ONR) tested the effectiveness of JABS as a mine neutralizer in the surf and beach zone. JABS transitioned to PMS-495 and the Navy fielded it as a non-material solution to an existing naval challenge. This method seems to be the ultimate in naval organic weaponry because every carrier and amphibious assault ship's strike aircraft can carry this weapon. The goal of current research at ONR is to extend the capability demonstrated in the surf and beach zones to the very shallow water (VSW). The new ONR program, called the Stand-Off Assault Breaching Weapon Fuze Improvement (SOABWFI) program, is testing the viability of JABS in water depths from 3.05 meters to 12.19 meters.

1. JABS

During the initial program, ONR concluded that JABS was competent in mine and obstacle clearance on the beach and in the surf zone (0 to 3.05 m). With accurate targeting information, it is effective, day or night, against unburied mines and obstacles in the surf and beach zones. Ultimately, it takes the man out of the minefield during neutralization (Almquist and McLaughlin 2008). Weaknesses include limited lethality against buried mines in the surf and beach zones, and a tail section that is more weakly constructed than the warhead resulting in tail fins or the whole tail section breaking off during initial water entry or during tail slap with the water cavity during its descent

through the water column (Almquist and McLaughlin 2008; Gefken 2006). JABS trajectory analysis showed that tail sensitivity is dependent on the impact angle of attack (AOA), defined here as the angle between the body axis and the velocity vector. If impact AOA is less than two degrees, the belief is that the tail will maintain structurally integrity beyond 28 msec. Above this limit, structural failure is likely (Watson et al. 2009).

2. SOABWFI

The SOABWFI program assesses the trajectory and the lethality of JABS in the VSW. Again, JABS consists of the 2,000-pound MK-84 general munition with the JDAM kit. The GBU-31 is the weapon's designation (Figure 4). It also gathers data on fuzing options and detonation times to analyze the weapon's lethality against various mines. If ONR is able to prove this concept, the Navy will have a truly organic capability to clear VSW mines with the standoff of up to about 15 nautical miles (Naval Air Weapons Center, Weapons Division 2002).

Figure 4. GBU-31(V)2 with MXU-735 nose cone [From NAVAIR 2009]

a. Evaluation of Precision-guided Bomb Trajectory through Water using Scale-Model Experiments

ONR contracted SRI International of Menlo Park, California to perform 19 scale model experiments to determine the trajectory of the MK-84 through the VSW. They used this data to predict maximum stable penetration depth, to gain insight on

required fuze delay time for optimum target lethality, and to estimate the final detonation position relative to the target position. The SRI report states that past research shows the water trajectory varies based on "initial velocity . . . and entry angle," so they looked closely at these specific parameters (Gefken 2006).

In order to examine correctly the MK-84 trajectory, they created four different configurations of the scale model to represent possible damage levels that may occur during water entry or because of tail slap within the cavitated region. The different configurations included a complete warhead section with (A) a tail section and four fins, (B) a tail section and two perpendicular fins, (C) a tail section and no fins, and (D) no tail section (Figure 5) (Gefken 2006).

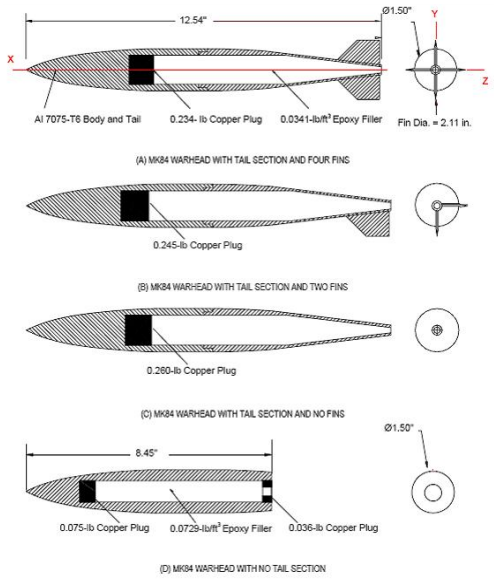

Figure 5. 1/12th scale MK-84 model design details [From Gefken 2006]

What SRI found during its experiment was that the tail section and fins play an important role in stabilizing the underwater trajectory (Figure 6). The more tail fins the bomb lost, the greater the increase in horizontal nose position, i.e., horizontal displacement from the point of water entry. When the weapon lost its tail altogether, it tumbled soon after water entry. They also noticed the weapons with a tail section had

similar overall trajectory shapes (single direction curve). Their results also showed that the horizontal displacement increased with increased impact velocity (Gefken 2006).

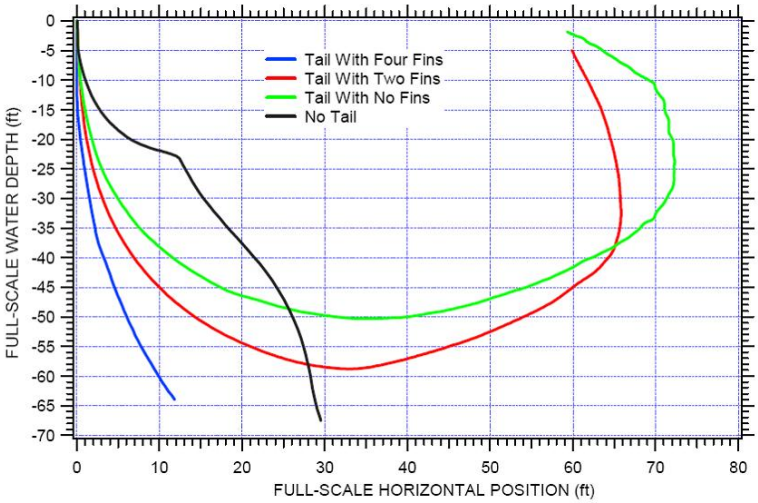

Figure 6. Trajectories for MK-84 warhead with different tail configurations [From Gefken 2006]

SRI confirmed that the bomb generated and traveled in a column of air (called cavitation) due to the high water-entry velocity during a majority of its underwater travel. In all 19 of their experiments, the cavitation generated in the water column consisted of:

> . . . a tapered cone that has a maximum full-scale diameter at the end of the tail section of about 3.0 ft. This is about a factor of two larger than the maximum bomb diameter of 1.5 ft. This cavity shape was about the same for all of the initial water-entry velocities [and bomb configurations] between 392 ft/s and 991 ft/s (Gefken 2006).

In this cavitated column, the pressure drag (produced by turbulent low-drag conditions down to a velocity of about 7.8 m/s for the scale model) dominates the dynamics of the bomb. Below this velocity, laminar flow dominates causing viscous forces on the body (Gefken 2006).

Due to the terminal velocity prior to detonation being greater than 7.8 m/s, the SRI report looked specifically at pressure drag. They found that the drag coefficient

(C_d) will vary depending on whether the trajectory is linear or curved. In the linear case, C_d is typically less than 0.1 for all tail configurations. For the curved trajectory, it is mostly between 0.2 to 0.3 with the bomb intact, but increases to 0.6 to 1.0 with two fins or tail without fins. Their data lastly indicates no correlation between a deviation of several degrees from a 90° water-entry angle and its ultimate trajectory (Gefken 2006).

The Reynolds number (Re) for the $1/12^{th}$ scale must equal the MK-84 Re in order for the scale model to represent an accurate depiction of the trajectory of the bomb. In this case, the Re's are not equal because of the inability to reduce the medium's kinematic viscosity by the scale factor. Instead, because the C_d tended to be very small in the region of turbulent flow, the assumption made was that the model provided a good simulation of the MK-84 for velocities above 7.8 m/s (Gefken 2006).

b. Underwater Bomb Trajectory Prediction for Stand-off Assault Breaching Weapon Fuze Improvement (SOABWFI)

The Naval Postgraduate School used the SRI data to create a 6 degree of freedom (6-DOF) computational bomb maneuvering model called STRIKE35. It predicts the trajectory, velocity, and orientation of a MK-84 inside the water column. In order to accomplish this, they found the diagnostic relationships using three momentum equations and three moment of momentum equations, and the relationship between the drag (C_d), lift (C_l), and torque (C_M) coefficients for the rigid body position and orientation. The basic dynamics of the model follows.

(1) Position and Orientation. The coordinate system, with the unit vectors (**i**, **j**) in the horizontal plane and (**k**) in the vertical direction, is earth-fixed. The bomb falling through the water column is assumed to be an axially symmetric rigid body where the head and tail coordinates are represented by $\mathbf{r}_h(t)$ and $\mathbf{r}_t(t)$, respectively. The unit vector representing the body's main axis direction (Figure 7) is **e**, where

$$\mathbf{e} = \frac{\mathbf{r}_h - \mathbf{r}_t}{\left|\mathbf{r}_h - \mathbf{r}_t\right|}. \tag{1}$$

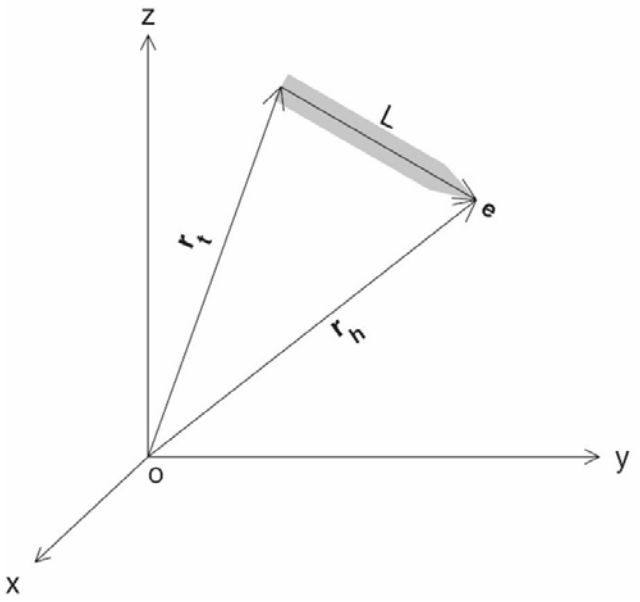

Figure 7. Position vectors (r_h, r_t) and the body axis unit vector (e) [From Chu et al. 2010]

In Figure 8, the center of mass (o_m) and center of volume (o_v) are located on the main axis, and the distance between them (σ) is positive (negative) when the direction from o_v to o_m is the same (opposite) as the direction of **e**. The lifting force and drag force (discussed in the next section) are $\mathbf{F}_l$ and $\mathbf{F}_d$, respectively. The angle of attack (α) is the angle between **e** and the unit vector of the rigid-body velocity ($\mathbf{e}_u$)

$$\alpha = \cos^{-1}(\mathbf{e}_u \bullet \mathbf{e}). \quad (1)$$

The angle between **e** and the horizontal plane is β

$$\beta = \sin^{-1}(\mathbf{e} \bullet \mathbf{k}), \quad (2)$$

and γ is the angle between $\mathbf{e}_u$ and the horizontal plane

$$\gamma = \sin^{-1}(\mathbf{e}_u \bullet \mathbf{k}). \quad (3)$$

In STRIKE35, the location of the body is represented by the position of o_m,

$$\mathbf{r}(t) = x\mathbf{i} + y\mathbf{j} + z\mathbf{k}. \quad (4)$$

The body velocity (also called translation) is then

$$\frac{d\mathbf{r}_o}{dt} = \mathbf{u}, \qquad \mathbf{u} = U\mathbf{e}_u, \tag{5}$$

where $(U, \mathbf{e}_u)$ are the speed and unit vector of the rigid-body velocity. Figure 9 shows the unit vector $\mathbf{e}_u$ broken into its components, $\mathbf{e}_u$, $\mathbf{e}_u^{\psi}$, $\mathbf{e}_u^{\gamma}$, $\mathbf{e}_u^{xy}$ where $\mathbf{e}_u^{xy}$ is the projection of $\mathbf{e}_u$ on the xy-plane

$$\mathbf{e}_u = \cos\gamma\cos\psi\mathbf{i} + \cos\gamma\sin\psi\mathbf{j} + \sin\gamma\mathbf{k} \tag{6}$$

where ψ is the azimuth and γ is the elevation angle. The unit vectors are also perpendicular to one another, $\mathbf{e}_u^{\psi} \perp \mathbf{e}_u$, $\mathbf{e}_u^{\gamma} \perp \mathbf{e}_u$, $\mathbf{e}_u^{\gamma} \perp \mathbf{e}_u^{\psi}$.

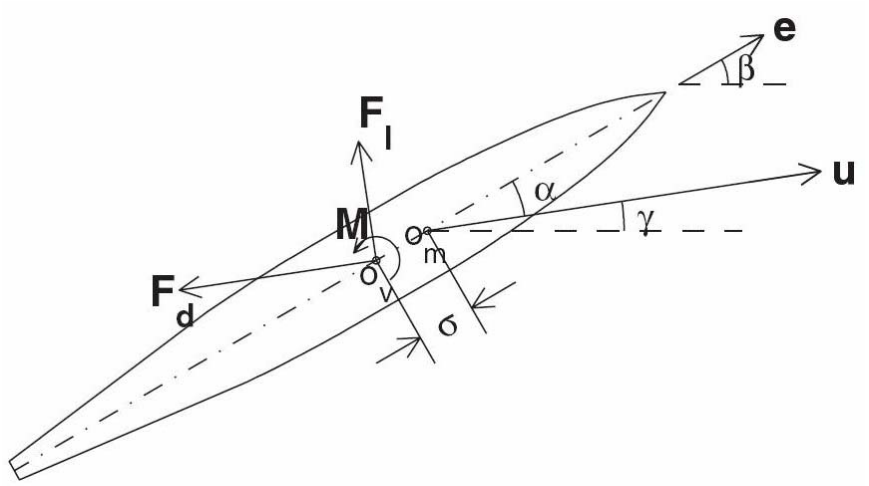

Figure 8. Angles, centers and forces of the bomb [Chu et al. 2010]

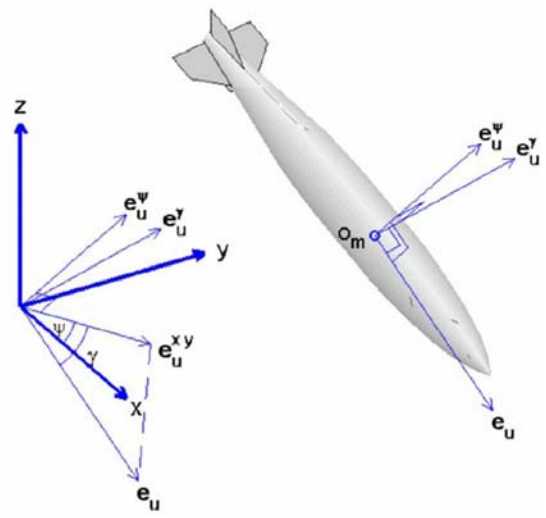

Figure 9. Unit vectors ($\mathbf{e}_u$, $\mathbf{e}_u^{\psi}$, $\mathbf{e}_u^{\gamma}$, $\mathbf{e}_u^{xy}$) [From Chu et al. 2010]

(2) Lift and Drag Coefficients. In order to define the lifting force, $\mathbf{F}_l$, they identify the unit vector ($\mathbf{e}_m^h$) as being perpendicular to both $\mathbf{e}$ and $\mathbf{e}_u$,

$$\mathbf{e}_m^h = \frac{\mathbf{e}_u \times \mathbf{e}}{|\mathbf{e}_u \times \mathbf{e}|}. \tag{7}$$

$\mathbf{F}_l$ is in the plane constructed by the vectors $\mathbf{e}$ and $\mathbf{e}_u$, and is in the same direction as $\mathbf{e}_m^h \times \mathbf{e}_u$ (i.e. perpendicular to both unit vectors). $\mathbf{F}_d$ is in the opposite direction of $\mathbf{u}$.

Both forces are exerted at o_v, and are described by

$$\mathbf{F}_d = -f_d \mathbf{e}_u \ , \ \mathbf{F}_l = f_l \mathbf{e}_l, \ \ \mathbf{e}_l = \mathbf{e}_m^h \times \mathbf{e}_u, \tag{8}$$

where f_d and f_l are the magnitudes of the forces. The lifting force is perpendicular to the drag force, and their magnitudes are represented by the drag law,

$$f_d = \frac{1}{2} C_d \rho A_w U^2, \ \ f_l = \frac{1}{2} C_l \rho A_w U^2. \tag{9}$$

Here, ρ is the density of water and A_w is the underwater projection area. C_d and C_l are the drag and lift coefficients that are determined by substituting the SRI position and orientation data into these theoretical diagnostic relationships and working backwards to statistically solve the semi-empirical formulas of the coefficients. Lastly, U is the water-

to-body relative speed. Because the water velocity ($\mathbf{V}_w$) is two orders of magnitude smaller than the bomb's velocity (**u**),

$$\mathbf{V} \equiv \mathbf{V}_w - \mathbf{u} \approx -\mathbf{u} = -U\mathbf{e}_u . \tag{10}$$

The bomb is a fast moving, rigid body with four fins that also have lift and drag components. In order to solve for these values simplistically, NPS assumes the fins are NACA0015 airfoils, which have known drag and lift coefficients. The additive effect of the combined drag and lift forces on a pair of fins (two fins in the same plane) is $\mathbf{F}_c^f$, so the total forces of the bomb's fins is $n\mathbf{F}_c^f$, where *n* is the number of fin pairs.

(3) Momentum Equation. Differentiating equation (5) with respect to time gives the acceleration of the rigid body,

$$\frac{d\mathbf{u}}{dt} = \frac{dU}{dt}\mathbf{e}_u + U\frac{d\mathbf{e}_u}{dt}. \tag{11}$$

This makes the momentum equation in the earth-fixed coordinate system

$$m\left(\frac{dU}{dt}\mathbf{e}_u + U\frac{d\mathbf{e}_u}{dt}\right) = \mathbf{F}, \tag{12}$$

where **F** is the resultant force consisting of

$$\mathbf{F} = \mathbf{F}_g + \mathbf{F}_b + \mathbf{F}_d + \mathbf{F}_l + n\mathbf{F}_c^f . \tag{14}$$

The gravity and buoyancy forces are

$$\mathbf{F}_g = -mg\mathbf{k}, \quad \mathbf{F}_b = \rho\Pi g\mathbf{k}, \tag{15}$$

where *m* is the bomb mass, *g* is gravity, and Π is the volume of the rigid body.

Computing the inner products between equation (12) and the unit vectors ($\mathbf{e}_u, \mathbf{e}_u^{\psi}, \mathbf{e}_u^{\gamma}$) for *n* = 0 leads to

$$m\frac{dU}{dt} = (\rho\Pi - m)g\mathbf{k}\bullet\mathbf{e}_u - f_d, \tag{16}$$

$$mU\frac{d\gamma}{dt} = \left[(\rho\Pi - m)g\mathbf{k} + f_l\mathbf{e}_l\right]\bullet\mathbf{e}_u^{\gamma}, \tag{17}$$

and

$$mU\cos\gamma\frac{d\psi}{dt} = \left[(\rho\Pi - m)g\mathbf{k} + f_l\mathbf{e}_l\right]\bullet\mathbf{e}_u^{\psi}. \tag{18}$$

The vector $\left[(\rho\Pi - m)g\mathbf{k} + f_l\mathbf{e}_l\right]$ is

$$\left[(\rho\Pi - m)g\mathbf{k} + f_l\mathbf{e}_l\right] = (m\frac{dU}{dt} + f_d)\mathbf{e}_u + mU\frac{d\gamma}{dt}\mathbf{e}_u^{\gamma} + mU\cos\gamma\frac{d\psi}{dt}\mathbf{e}_u^{\psi}. \tag{19}$$

Because $m\frac{dU}{dt} + f_d$ is in the $\mathbf{e}_u$-direction, $mU\frac{d\gamma}{dt}$ is in the $\mathbf{e}_u^{\gamma}$-direction, and $mU\cos\gamma\frac{d\psi}{dt}$ is in the $\mathbf{e}_u^{\psi}$-direction, they used the perpendicularity condition and the inner product of (19) by the unit vector $\mathbf{e}_l$ to calculate

$$\left[(-m + \rho\Pi)g\mathbf{k} + f_l\mathbf{e}_l\right]\bullet\mathbf{e}_l = \left[mU\frac{d\gamma}{dt}\mathbf{e}_u^{\gamma} + mU\cos\gamma\frac{d\psi}{dt}\mathbf{e}_u^{\psi}\right]\bullet\mathbf{e}_l. \tag{20}$$

(4) Moment of Momentum Equation. The moment of momentum equation, relative to o_m, is

$$\mathbf{J}\bullet\frac{d\mathbf{\Omega}^*}{dt} = \mathbf{M}_b + \mathbf{M}_h. \tag{21}$$

Here **J** is the gyration tensor, which is a diagonal matrix in the body-fixed coordinate system,

$$\mathbf{J} = \begin{bmatrix} J_1 & 0 & 0 \\ 0 & J_2 & 0 \\ 0 & 0 & J_3 \end{bmatrix}. \tag{22}$$

J_1 , J_2, and J_3 are the moments of inertial, and for an axially symmetric, rigid body J_2 and J_3 are equal. The rotation velocity of the rigid body is

$$\frac{d\mathbf{\Omega}^*}{dt} = \frac{d\Omega_s}{dt}\mathbf{e} + \Omega_s(\mathbf{\Omega}\times\mathbf{e}) + \frac{d\mathbf{\Omega}}{dt}, \tag{23}$$

where $\mathbf{\Omega}^*$ is the rigid body's angular velocity vector, and its components are the bank

angle (Ω_s) along the unit vector **e,** and the other azimuthal and elevation angles perpendicular to **e** ($\boldsymbol{\Omega}$). The torque by the buoyancy force (or buoyancy torque) is

$$\mathbf{M}_b = -\sigma\mathbf{e}\times\left(\rho\Pi g\mathbf{k}\right). \tag{24}$$

Lastly, the hydrodynamic torque ($\mathbf{M}_h$), relative to o_m, is computed

$$\mathbf{M}_h = -\sigma\mathbf{e}\times(\mathbf{F}_d+\mathbf{F}_l) - n\sigma_f\mathbf{e}\times\mathbf{F}_c^f + \mathbf{M}_{tr} + \mathbf{M}_{rot}. \tag{25}$$

Here $\mathbf{M}_{tr}$ is the anti-translation torque by the moment of drag and lift forces and $\mathbf{M}_{rot}$ is the antirotation torque, which is dependent on the Re. With a little manipulation and the assumption that this rigid-body has very slow or no self spinning ($\Omega_s \simeq 0$), the component of the moment of momentum equation that is perpendicular to **e** is

$$\mathbf{J}_2\bullet\frac{d\boldsymbol{\Omega}}{dt} = \hat{\mathbf{M}} \equiv -\sigma\rho\Pi g\mathbf{e}\times\mathbf{k} - \sigma\left(f_d\mathbf{e}\times\mathbf{e}_u + f_l\mathbf{e}\times\mathbf{e}_l\right) - n\sigma_f f_c^f\mathbf{e}\times\mathbf{e}_c^f + \mathbf{M}_{tr} + \mathbf{M}_c. \tag{26}$$

(5) Hydrodynamic Coefficients. Ultimately, they rewrote the coefficients as

$$C_d = \frac{2[(\rho\Pi - m)g\mathbf{k}\bullet\mathbf{e}_u - m\frac{dU}{dt}]}{\rho A_w U^2}, \tag{27}$$

$$C_d = \frac{2[mU(\mathbf{e}_u^{\gamma}\frac{d\gamma}{dt} + \mathbf{e}_u^{\psi}\cos\gamma\frac{d\psi}{dt})\bullet\mathbf{e}_l - (\rho\Pi - m)g\mathbf{k}\bullet\mathbf{e}_l]}{\rho A_w U^2}, \tag{28}$$

and

$$C_m = \frac{J_2\frac{d\boldsymbol{\Omega}}{dt}\bullet\mathbf{e}_m^h + \sigma\rho\Pi g(\mathbf{e}\times\mathbf{k})\bullet\mathbf{e}_m^h}{\frac{1}{2}\rho A_w L_w U^2} + CF(\boldsymbol{\Omega}\frac{L_w}{V_r})\frac{V_r^2}{U^2}\cos\gamma\frac{d\psi}{dt})\mathbf{e}_{\omega}\bullet\mathbf{e}_m^h + \frac{\sigma}{L_w}[C_d(\mathbf{e}\times\mathbf{e}_u)\bullet\mathbf{e}_m^h + C_l(\mathbf{e}\times\mathbf{e}_l)\bullet\mathbf{e}_m^h]$$

(29) (Chu et al. 2010).

(6) STRIKE35 Verification with 1/12th Scale MK-84 Models. STRIKE35 uses the Boeing Corporation's specifications data of the full-scale MK-84 (length, mass, mass inertia properties) for all variants (four, two, and no fin, as well as no tail). It solves the momentum equations and the moment of momentum equation using the numerical method and the derived hydrodynamic coefficients. Successful verification occurred by inputting the SRI configuration, water impact speed, and impact angle data to compare the STRIKE35 predicted trajectory and orientation to the observed SRI runs (Figures 10 through 13) (Chu et al. 2010).

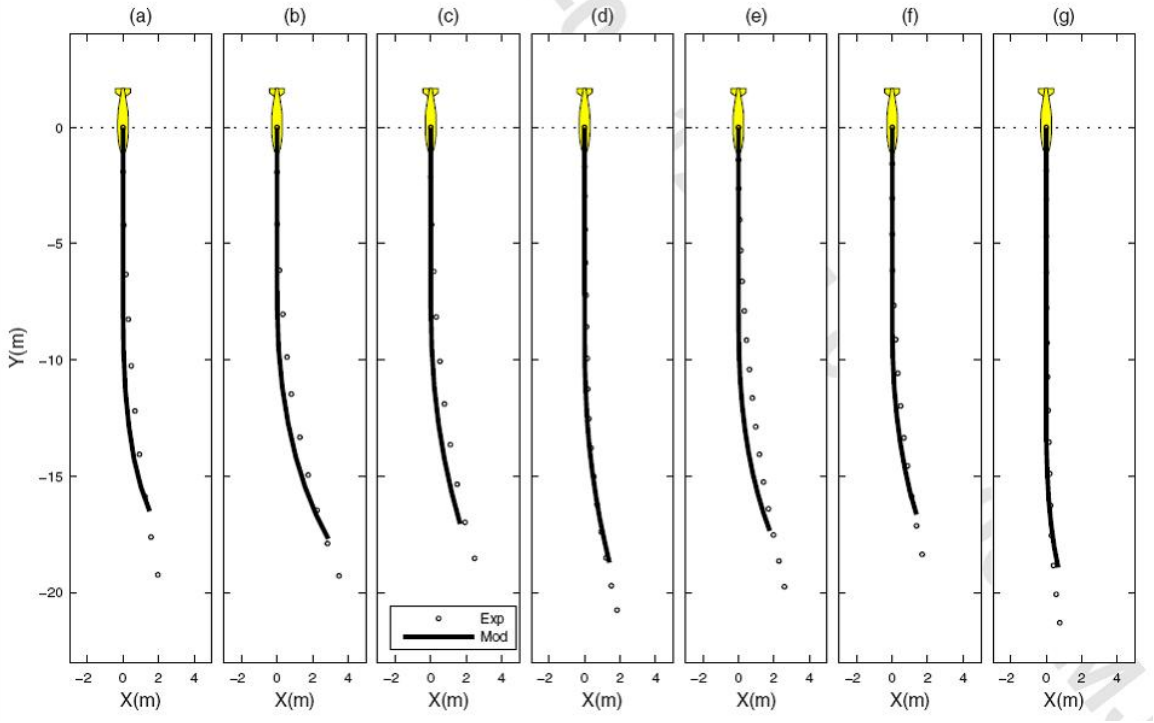

Figure 10. Trajectory comparison of predicted and observed MK-84 with tail and four fins with initial water entry conditions: (a) 132 m/s and 0.8° AOA, (b) 297 m/s and 0° AOA, (c) 295 m/s and 1.2° AOA, (d) 302 m/s and 1.5° AOA, (e) 227 m/s and 2° AOA, (f) 219 m/s and 1° AOA, and (g) 119 m/s and 1.8° AOA [From Chu et al. 2010]

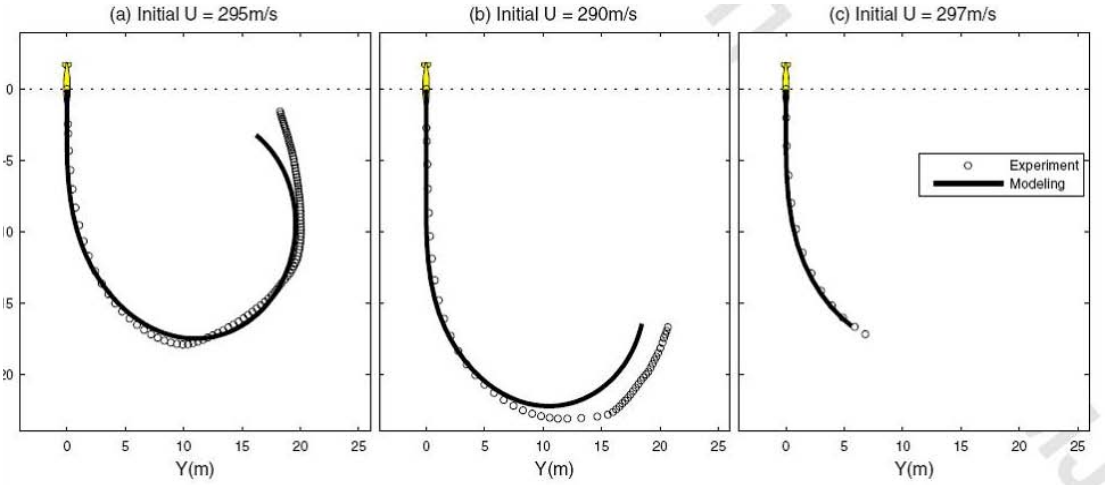

Figure 11. Trajectory comparison of predicted and observed MK-84 warhead with two fins and initial water entry conditions: (a) 295 m/s and 0° AOA, (b) 290 m/s and 0° AOA, and (c) 297 m/s and 0° AOA [From Chu et al. 2010]

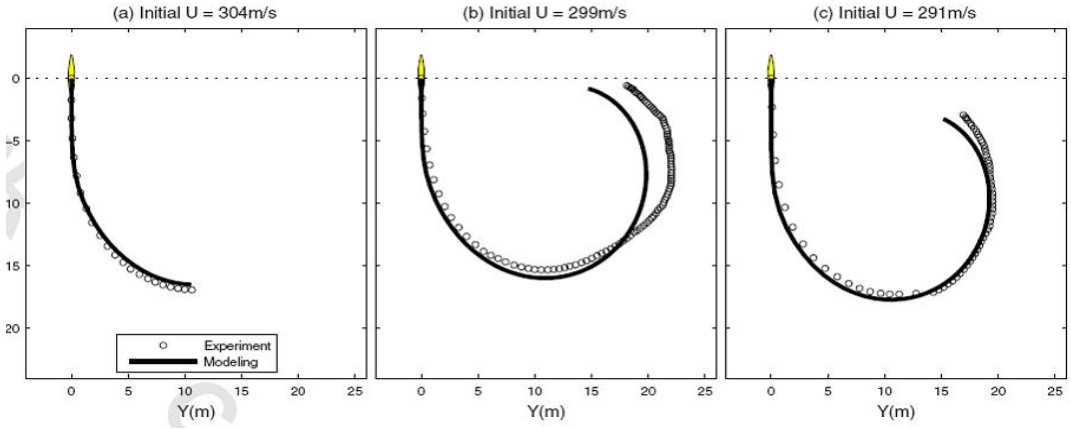

Figure 12. Trajectory comparison of predicted and observed MK-84 warhead with tail section and no fin with initial water entry conditions: (a) 304 m/s and 0° AOA, (b) 299 m/s and 3° AOA, and (c) 291 m/s and 1.9° AOA [From Chu et al. 2010]

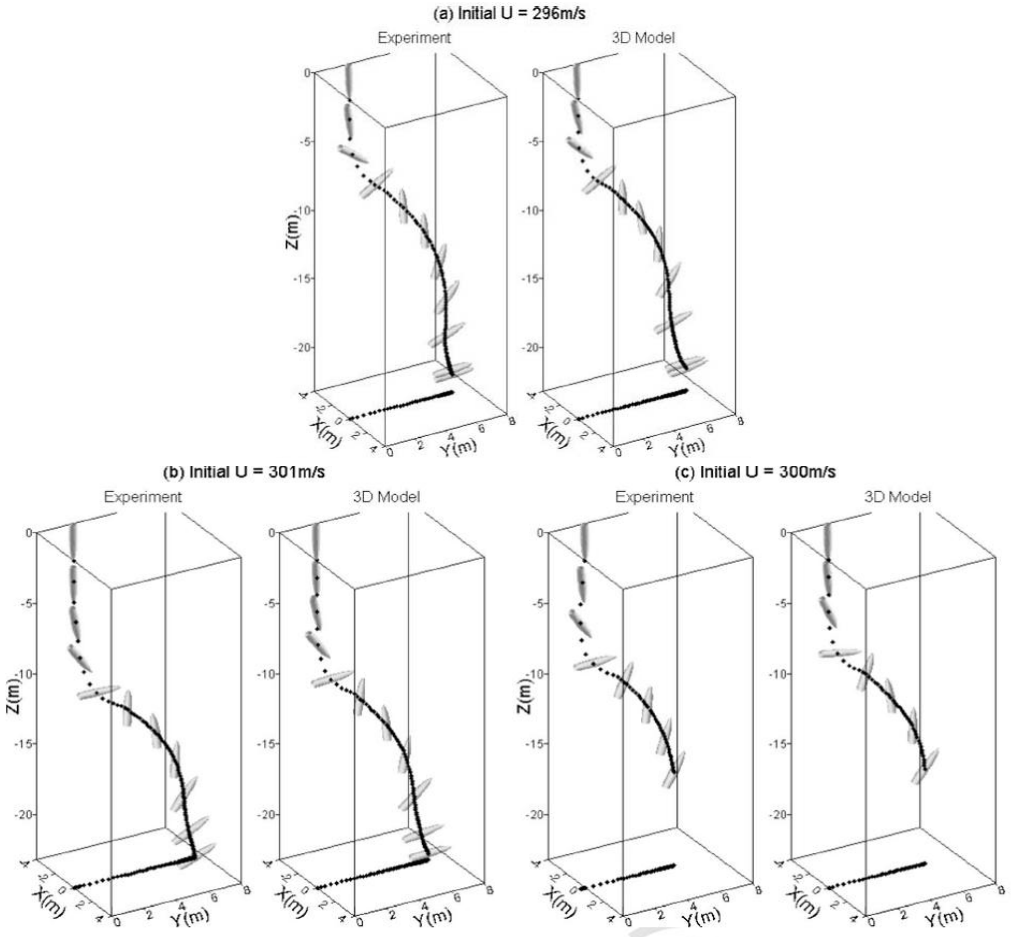

Figure 13. Trajectory comparison of predicted and observed MK-84 warhead with no tail section and initial water entry conditions: (a) 296 m/s and 4.3° AOA, (b) 301 m/s and 0° AOA, and (c) 300 m/s and 1.3° AOA [From Chu et al. 2010]

The paper on the creation of STRIKE35 concludes that C_d and C_l depend less on Ω and more on Re and AOA. They found that C_d increases with Re, for constant AOA. Holding Re constant, C_d monotonically increases with AOA from vertical to a horizontal drop (0 to 90° AOA). The C_m depends only on Re and AOA. C_l also depends on Re and AOA, but the reliance is more complicated (Chu et al. 2010).

B. CURRENT ANALYSIS

The creation and verification of STRIKE35 used the same data. As seen in Figures 10–13, the trajectory of the scaled down MK-84 is represented well using the computer model. This thesis amends STRIKE35 in order to validate the program's physics for live and inert GBU-31s dropped into a 7.62 m and 12.2 m test ponds. With the newly verified model, we solve for the limiting impact AOA and impact speed to remain within a Technology Transfer Agreement (TTA) requirement. Last, this thesis finds the limiting impact AOA and impact speed for all the delay settings, to include the 20% tolerance in the weapon specification document, in the FMU-139 fuze in an ocean environment (Boeing 2009).

By knowing the underwater trajectory of a GBU-31, the Navy can usefully employ this truly organic, proven warhead efficiently and effectively to quickly clear a minefield without harming people or trained marine mammals. The JDAM is a joint asset that can neutralize a mine any time of day and in any weather condition. This thesis provides an accurate, cost effective tool for determining the final detonation position relative to the water impact location.

THIS PAGE INTENTIONALLY LEFT BLANK

III. SOABWFI FLIGHT TESTING

A. TEST PREPARATION AND PROCEDURES

1. Test Ponds and Targets

Naval Air Warfare Center, Weapons Division (NAWC/WD) created two circular ponds in the middle of Indian Wells Valley, California (Figure 14). They are built the same, both having a circular bottom with a diameter of approximately 30.5 m, except for the depths. The smaller pond is about 7.6 m deep and the larger is about 12.2 m deep. Sloping sides (2:1) create a surface diameter of roughly 61 m for the smaller pond and 79 m for the larger diameter. Both ponds have a ramp built into the side for vehicle access. A plastic liner covers the dirt to contain the brackish water (Figure 15) that is supplied by a 206 m deep, on-site well that filled both ponds at about 800 gallons per minute (Figure 16) (Watson et al. 2009). Placed inside the water are fully operational, moored, foreign mines filled with simulant, instead of TNT. Their nomenclature is "JV" as to avoid classification issues.

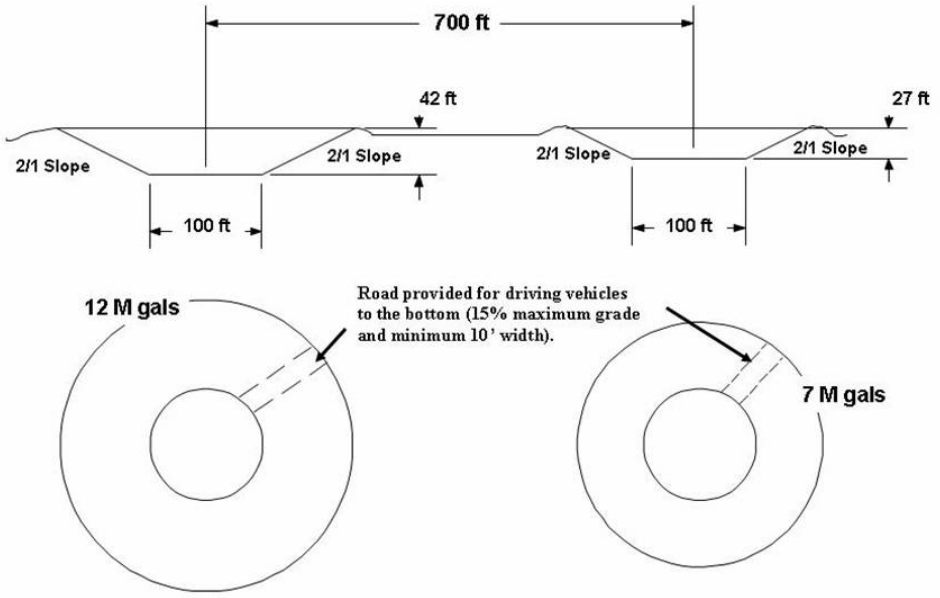

Figure 14. Artificial ponds used for the flight tests at NAWC/WD [From Watson et al. 2009]

Figure 15. (a) Man-made lake (approximately 7.6 m deep) covered in plastic with the side road (b) and four JV mines [From Thomas Kelsh 2009]

Figure 16. Ground water from a PVC pipe fills the test pond

2. Instrumentation

These experiments use two types of high-speed digital cameras, light sensors, pressure sensors, and a global positioning system (GPS) to collect the data. The range cameras capture 60 frames per second and the two Phantom cameras capture 1,000 frames per second. From the shore of the pond, they collect data that assists in solving for the location, speed, and orientation of the weapon at the time of water impact (Figure 17). Using orthogonal images from the Phantom cameras, they could also solve for the water impact AOA. The light and pressure sensors provide the time and depth of detonation for the inert weapons equipped with a fuze and booster. The booster fires at

the same time as the fuze, sending out a pressure pulse and light flash that is picked up by the sensors. This, of course, assumes that the speed of light is infinite and pressure translates short distances almost instantaneously in incompressible fluid (Boeing 2009a). The horizontal displacement of the weapon in the pond is determined by comparing the distance between the water impact and pond bottom impact. The camera images help solve for the water location and the Trimble 5800 GPS system locates the pond bottom impact location surveying the holes (Figure 18) (Watson et al. 2009).

Figure 17. High speed digital camera

Figure 18. GPS surveys impact holes [From Boeing 200b]

Though the image quality of the Phantom cameras is superior to the range cameras, their orientation accuracies are unknown due to their non-surveyed placement.

Preliminary findings from Underwater Trajectory Test Three (UTT-3) state that the vertical axis alignment is good to only about 2°, making it unlikely to find absolute measurements of body axis angle or velocity vector direction at impact. Absolute errors in the camera measurements cancel out when looking at the differences between the two, though. Therefore, the AOA (defined here as the difference between the body axis angle and the velocity vector) is the accurate comparison between the individual analyzed runs (Boeing 2009c).

3. Aircraft and Weapons

An F/A-18F Super Hornet, proceeding at 0.80 Mach, dropped live and inert GBU-31s from 35,000 feet mean sea level (MSL). Release occurred approximately 5–7 miles from the pond in order to give the glide weapon enough kinematic energy to orient itself vertically above the designated point of impact (DPI). The desire is to have the velocity vector aligned with the munitions axis (zero AOA), and both vectors perpendicular to the flat, water surface. All of the GBU-31s penetrated the water within the prescribed delivery error of less than 2 m Circular Error Probable (CEP) at velocities between 382.5 and 394.9 m/s.

Every JABS in the experiments had the MXU-735 nose cone and the tail telemetry (TM) kit installed. The nose cone is blunter than the Navy's Ogive nose used in previous experiments (Figure 19). The flatness forces a larger cavitation tunnel for the weapon to proceed through. The TM provides data, via line of sight transmission, on various flight parameters such a velocity, heading, altitude, and angle of attack. Since there is not a line of sight from the pond to range control, the TM's lowest data transmission was about 32.9 m above the pond.

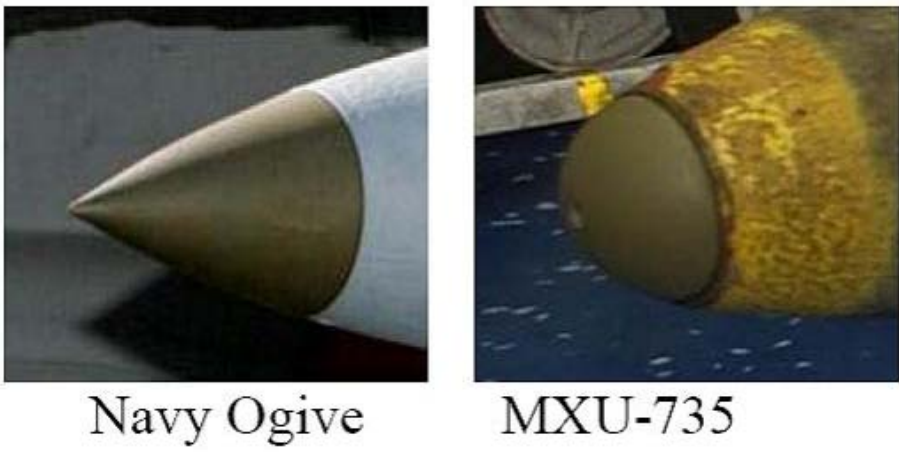

Figure 19. Differing nose cones between JABS and SOABWFI [From Boeing 2009c]

The weapons that had fuzes were equipped with an FMU-139 B/B with available delay settings of 0, 10, 25, and 60 msec. Selection of the delay depends on which types of targets the weapon is to attack. The explosive in the live weapon is PBXN-109, whereas the inert weapons have filling to maintain appropriate weight and balance.

B. UNDERWATER TRAJECTORY TEST ONE (UTT-1)

The following description includes all that is not standard about the first Underwater Trajectory Test of the SOABWFI program. The primary purpose of this experiment was to collect data to measure the underwater trajectory deviation of the JABS traveling through 7.62 m of water. A secondary objective was to obtain information to help characterize the error budget in fuze delay, which is nominally ±20% according to the weapon specification document (Boeing 2009b).

On August 7, 2008, the Super Hornet dropped four inert GBU-31s into the shallow pond. The delivery error, defined as the (x, y) distance between the DPI and the actual weapon impact point, averaged 1.3 m in this test. Three of the four weapons were equipped with a live FMU-139 fuze (and booster) set for a 10 msec delay, though the sensors internal to the pond failed to detect the flash of light and pressure pulse caused by the fuze booster (Boeing 2009b).

A repeater was not available for retransmission of the TM signal to range control, so the last receipt of the line of sight signal was at best 32.9 m above the pond. TM data was able to confirm that the mission planning for the target elevation was incorrectly set for 7.62 m below the bottom of the pond instead of the desired 7.62 m above (at the water surface). This human error likely introduced some uncorrected weapon AOA at water impact; this is because the weapon sets the programmed AOA directly before impact, but the weapon also thought it had 15.24 m of descent left to set the AOA (Boeing 2009b).

Table 2 shows that only two of the bombs have complete water impact information. For the first drop, the last known velocity was at about 2.0 km above ground level. The other three drops, in order, had TM data for 32.9, 55.5, and 78.0 m above the pond (Boeing 2009a). The fourth drop had one of the Phantom cameras fail. Typically solving for the AOA takes two orthogonal vectors. We know the total AOA must be greater than the largest component and smaller than the sum of the components. From this, we know that having only one vector we can only solve for the lower bound (Boeing 2009b). Although they made no effort to find and catalog debris from the weapons, there was some evidence that at least two fins came off (Boeing 2009b).

Run	Impact Velocity (m/sec)	Angle of Attack (degrees from horizontal, ±0.5 degrees)	Total Nose Displacement (m from surface impact)	Final Nose Depth (m)
1	unk	1.66	0.11	25
2	389.4	1.44	0.66	25
3	388.2	1.59	0.56	25
4	388.8	$\geq$1.91	0.57	25

Table 2. UTT-1 known characteristics

C. LIVE FIRE FLIGHT DEMONSTRATION ONE (LFFD-1)

On September 9, 2008, the first live fire demonstration of the JABS against mine-like (JV) targets occurred at the shallow pond. Because of an incorrect fuze delay setting

(human error; zero was set), the bomb detonated prematurely. The test results were invalid because the weapon detonated very shortly after impact. A duplicate assessment (LFFD-1 Repeat) then occurred on November 19, 2008 with satisfactory results; the description below is all that is non-standard about the repeat test (Boeing 2009a).

The primary purpose of the experiment was to demonstrate the lethality of one GBU-31 against several mine threats normally found at 7.62 m water depth, which are generally different from those previously tested during JABS. A secondary objective was to obtain pressure measurements in order to measure the explosive output and correlated damage to the targets. Since the pressures and correlating damage are incidental to this thesis, as well as classified, the forthcoming analysis will not discuss them (Boeing 2009a).

The circle in Figure 20 represents the flat bottom of the small pond with the DPI at the center (0, 0). Plotted on this figure are the locations of the LFFD-1 test mines with East in the positive x direction and North in the positive y direction (m). Two mines, located at (0, ±7.3), had a maximum predicted neutralization distance of 15.2 to 18.3 m by the JABS. Two mines, located at (±9.8, 0), had a maximum predicted neutralization distance of over 30.5 m by the JABS. The remaining three mines, at standoff distances of 3.0, 4.6, and 6.1 m from the center (2.1, -2.3), (3.5, 3.1), and (-5.6, 2.2), are typically found at 4.6 m of water and have a maximum neutralization distance of 6.1 to 9.1 m by the JABS at this lesser depth (Boeing 2009a).

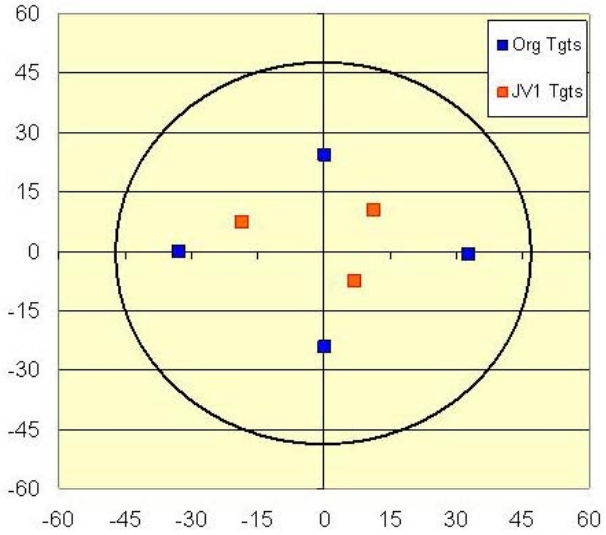

Figure 20. Horizontal positions of JV mines in the pond [From Boeing 2009a]

Analyzing the NAWC/WD camera data, the weapon hit the pond within a few meters (1.3, -0.6) of its DPI (0.0, 0.0). Unlike the first LFFD-1, this weapon detonated approximately 12 msec after impact (Figure 21). Post explosion, the lake had lost approximately 0.9 m of water, and a grey film sat on the perimeter (Figure 22). Large pieces of debris were outside of the pond, some as far as 30.5 m away from the edge (Figure 23). Visual inspection of the JV mines showed damage, and draining the pond (Figure 24) revealed a large, bottom crater, presumably caused by the effect of the bubble expansion seen in Figure 21, frames three through six (Boeing 2009a).

Figure 21. Detonation sequence [From Boeing 2009a]

Figure 22. Post detonation test pond

Figure 23. Test pond debris

Figure 24. Drained test pond

Table 3 shows the repeat test's pertinent water impact characteristics. Using a software program called LOCATE, the Naval Surface Warfare Center, Carderock (NSWC/CD) solved numerical equations for the weapon position and time at detonation. An assumption made to calculate this position was that the center of the charge was approximately at the center of the 2.4 m long explosive section, which is about 1.2 m from the tip of nose. Results for the position at detonation are (1.5, -0.6, -3.1) m. The detonation x- and y-coordinates are very close to the impact position (1.3, -0.6, 0.0) m. Based on the digital imagery, the actual time of detonation was 12 msec (Boeing 2009a). Using the Pythagorean Theorem to calculate the actual travel distance of 3.6 m, we find the detonation time and distance correlates well: (382.5 m/sec)(0.012 sec) = 4.59 m (nose) – 1.2 m (explosive) = 3.39 m. This does not account for the deceleration of the weapon penetrating the water, but allows the reader to see that the assumptions made still compute to a reasonable error of 0.21 m.

Run	Impact Velocity (m/sec)	Angle of Attack (degrees from horizontal, ± 0.5 degrees)	Total Explosive Displacement (m from surface impact)	Final Explosive Depth (m)	Time to Detonation (sec)
1	382.5	2.04	0.18	3.1	0.012

Table 3. LFFD-1 known characteristics

D. UNDERWATER TRAJECTORY TEST TWO (UTT-2)

The subsequent explanation is the non-standard occurrences from the second Underwater Trajectory Test of the SOABWFI program, which took place in the deep pond. The primary purpose of this experiment was to collect data to measure the underwater trajectory deviation of the JABS traveling through 12.2 m of water. A secondary objective was to evaluate the fuze function with a 25 msec delay, and collect pressure data during the underwater trajectory (Boeing 2009c).

On February 28, 2009, the Super Hornet dropped two inert GBU-31s into the deep pond. The original plan was to drop four, but the third weapon hung on the bomb

rack, requiring the pilot to execute hung ordnance procedure. This ultimately terminated the flight without dropping the last two bombs. A strong wind event had occurred the previous day, so the depth of the pond was about 11.9 m. During the two drops, the wind averaged 1.5 m/s, which was too low to have had a major impact on the weapons' AOA. The average delivery error of the two drops was 1.5 m. As well, the second weapon had a live FMU-139 fuze (and booster) set for a 25 msec delay (Boeing 2009b).

This experiment included four towers each with four underwater video cameras, which recorded (at 60 frames per second) the first drop aimed at the West aim point (AP) (Figure 25). These video images clearly show this weapon did not continue straight beyond about 6 m depth. In fact, they show evidence that the tail of the weapon hit the cavity wall when the nose was about 5.5 m depth and broke off at least a piece of it (Figure 26). It is clear that the interior of the tail section was fully exposed to the water, but unclear from the photos if the tail separated fully from the body before bottom impact (Boeing 2009b).

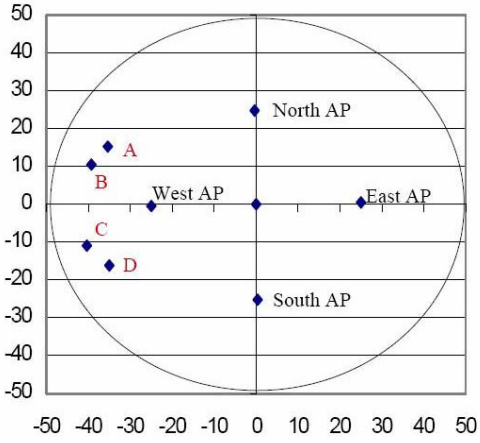

Figure 25. Aim points (AP) and camera towers [From Boeing 2009b]

Figure 26. Tower A, camera 2 images showing tail parts leaving the cavity (sequential photos with 66 msec between) [From Boeing 2009b]

Table 4 shows the second underwater trajectory test's pertinent water impact characteristics. Both weapons had such an angle when hitting the pond's bottom that it was difficult to locate where the nose first penetrated the pond bottom. To reconstruct where the hole was located in the plastic liner, to within 0.3 m accuracy, they had the liner extracted and stretched out. The second weapon, aimed at the North AP, hit the bottom with shallow enough angle to burrow under the liner, climb the North pond face for a bit before re-entering the water going upwards, and finally getting airborne (Figure 27).

Figure 27. UTT-2(2) get airborne after penetrating the pond bottom [From Boeing 2009b]

Run	Impact Velocity (m/sec)	Angle of Attack (degrees from horizontal, ±0.5 degrees)	Total Nose Displacement (m from surface impact, ± 0.3 m)	Final Nose Depth (m)
1	392.2	1.27	0.72	39.1
2	394.9	2.27	0.43	39.1

Table 4. UTT-2 known characteristics

IV. MODEL VERIFICATION USING JDAM AND APPLICATION

A. OVERVIEW

As the SRI experiment reported, the bomb moves at a high velocity through the water and flow separation creates a cavity of air around the body. That cavity, sometimes called cavitation, then remains in the water long after the bomb has passed and causes two areas of concern. First, will the trajectory remain stable, or will it tumble inside its own air cavity? Second, when the bomb does hit the cavitation wall, will the tail fins break? In addition, what happens to the trajectory after the fins break (Boeing 2009c)?

Currently, three tests are available from which to draw data, as seen in Tables 2 through 4. All three prove stability of the weapon to a certain depth in the water column, regardless of tail or fin separation. They also show that the tail fins most likely do (and the tail section possibly does) not remain intact during the full descent to the pond's bottom, regardless of the impact AOA.

According to the Boeing report (2009c), they found tail fin debris at the bottom of both UTT ponds. Though no underwater camera was available for UTT-1, once they drained the pond there was evidence that at least two tail fins came off the weapons. During UTT-2, camera images are only available for the first drop. They strongly suggest the first weapon's tail impacted the cavity wall when the tail was about 1.5 m below the surface (the nose was around 5.5 m in depth), starting the process of breaking pieces off of the tail section, ultimately separating all four tail fins from the body.

There is evidence that the second bomb also lost its fins. The SRI experiment shows that a bomb without tail fins is stable, but has significant curvature during its trajectory through the water. In the case of UTT-2(2), the bomb penetrated the bottom at such a shallow angle that it was able to burrow under the pond liner, climb the North face of the pond wall for a distance, re-enter the water traveling upward, and subsequently get airborne again (Boeing 2009c). This is a strong indicator that the bomb's tail fins broke off far enough above the bottom of the pond to allow it to turn in the water. If this

shallow angle hypothesis is true, how is it that there is only a small horizontal deviation between the surface impact point and the bottom impact point? The following sections will explain.

B. MODEL VERIFICATION

1. Lifting Surface Area Estimate

STRIKE35 was created and tested on 1/12th scale replicas of the MK-84, so we must verify if the physics hold true for the full scale GBU-31, as well. As previously stated, there is only one model run that has the possibility of having maintained all four of its tail fins at a measurable point. LFFD-1 shows the best possibility of validating STRIKE35 because it traversed either without broken tail fins or the least distance with broken tail fins. An unknown, at the time of this validation, was the surface area of the lifting surfaces (tail fin and aero-surfaces or strake) (Figure 28). Known information about this drop is in Table 3. Another known fact is that STRIKE35 places the lifting surfaces solely at the tail section, so the validation needs to make up for this difference by changing the surface area of the tail fin in the model.

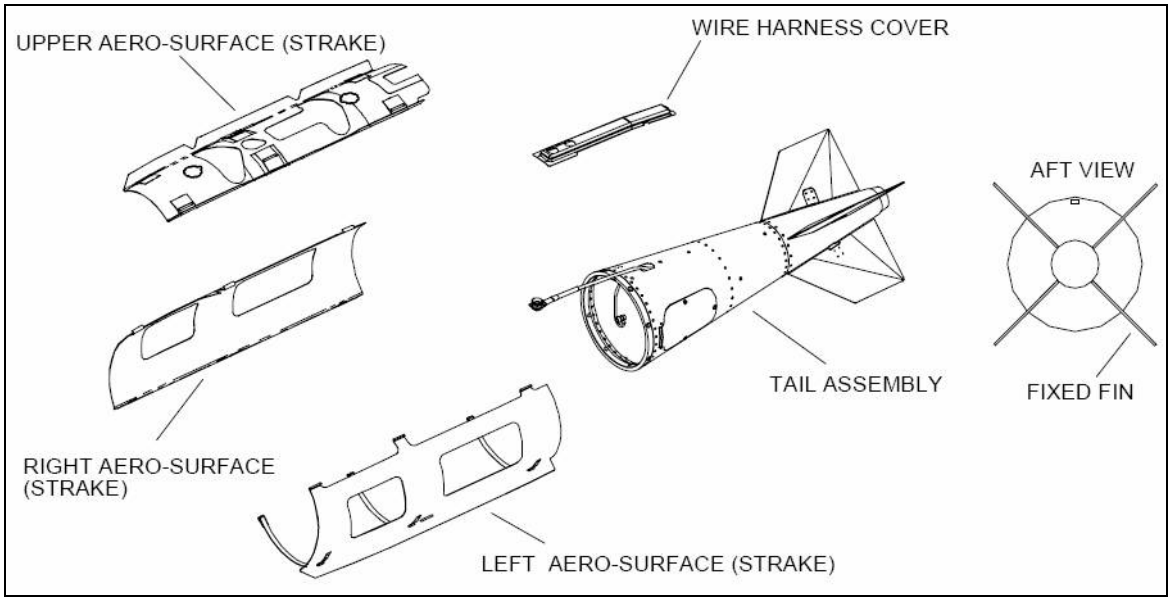

Figure 28. GBU-31(V)2/B guidance set (U) [From Naval Air Weapons Center, Weapons Division 2002]

Because the data captured in LFFD-1 showed that the detonation occurred 12 msec after water impact, so all lifting area comparisons were at 12 msec. Adjustments to the size of the fin surface area enabled an evaluation between the observed detonation horizontal deviation and the STRIKE35's position. After changing the surface area of the fin and running the model, the nose and center of mass points helped solve for the equation of the body axis line. The known nose depth at detonation was plugged into the equation to solve for the horizontal displacement of the STRIKE35 weapon's nose. The most accurate surface area, 0.68 m^2, brought the model within 6.8% of LFFD-1's observed horizontal deviation, which is within the measurement uncertainty (Figure 29). This is much larger than the actual area of a tail fin pair (two tail fins in the same plane) and the aero-surfaces (strakes) combined (later found to be about 0.264 m^2), but as a correction factor it works well as seen in the forthcoming validation.

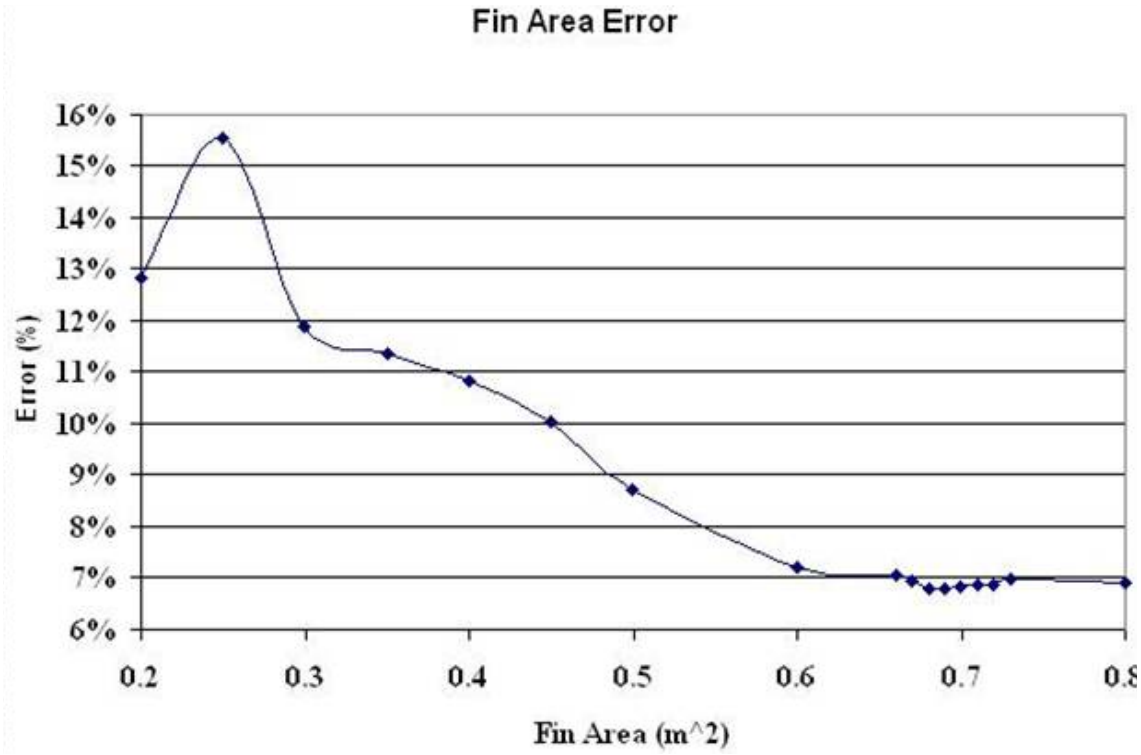

Figure 29. The most accurate depiction of LFFD-1: single fin surface area of 0.68 m^2

Calculating the accuracy for each "fin surface area" type is as follows. The displaced location, meaning the horizontal distance from initial water impact to the

detonation point, of the LFFD-1 weapon was 0.183 m from the point of water impact. In order to compare the STRIKE35 run (fin area of 0.68 m^2), we found the equation of the line between the nose coordinate (0.4089, -4.048) m and the center of mass (0.04197, -2.487) m to be y = -4.2542x – 2.3085 (Figure 30). Plugging the detonation depth (y = 3.14 m) in to this equation gives the calculated horizontal displacement (x) of the nose as 0.195 m. This case is the least distance (0.012 m) between the observed and STRIKE35 horizontal displacement. The error is the absolute value of the difference between the observed and the modeled horizontal deviation from water impact, all over the observed horizontal deviation (6.8%).

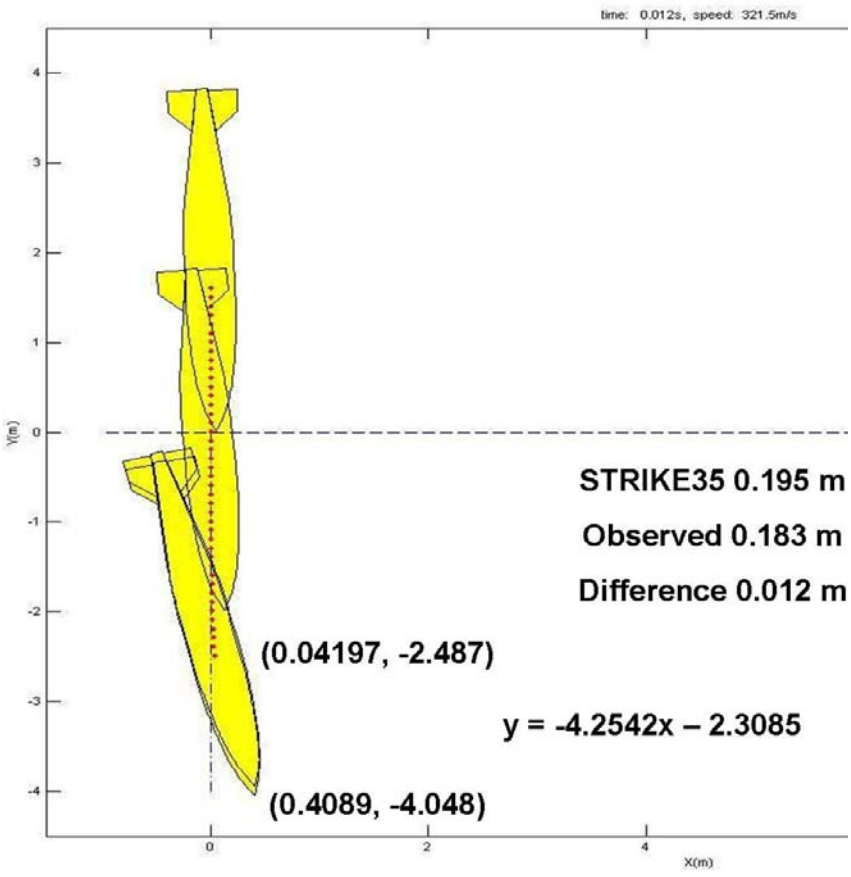

Figure 30. LFFD-1 with 0.68 m^2 single fin surface area

2. Verifying Tail Breakage Physics of the Model

Utilizing this adjusted fin area model, we ran all four of the remaining complete data sets (Tables 2 and 4) assuming the tail fins remained intact (Figures 31 through 34, respectively). All of the STRIKE35 runs were within one foot of the observed horizontal displacement, so it would seem that the weapons might have retained all four tail fins. However, there is strong evidence to the contrary. After draining the UTT-1 pond, pieces of tail fin were at the bottom. We also know that during UTT-2(1) some of the tail fins definitively did not remain on the weapon. The underwater video cameras captured tail fin pieces leaving the cavitation wall when the nose was at a depth of about 5.5 m. Lastly, we saw in the SRI experiment that fewer tail fins caused more curvature in the weapon's underwater trajectory; due to both UTT-2 weapons penetrating the deep pond's bottom at a significant angle from vertical, this also lends to the hypothesis that both weapons lost tail fins.

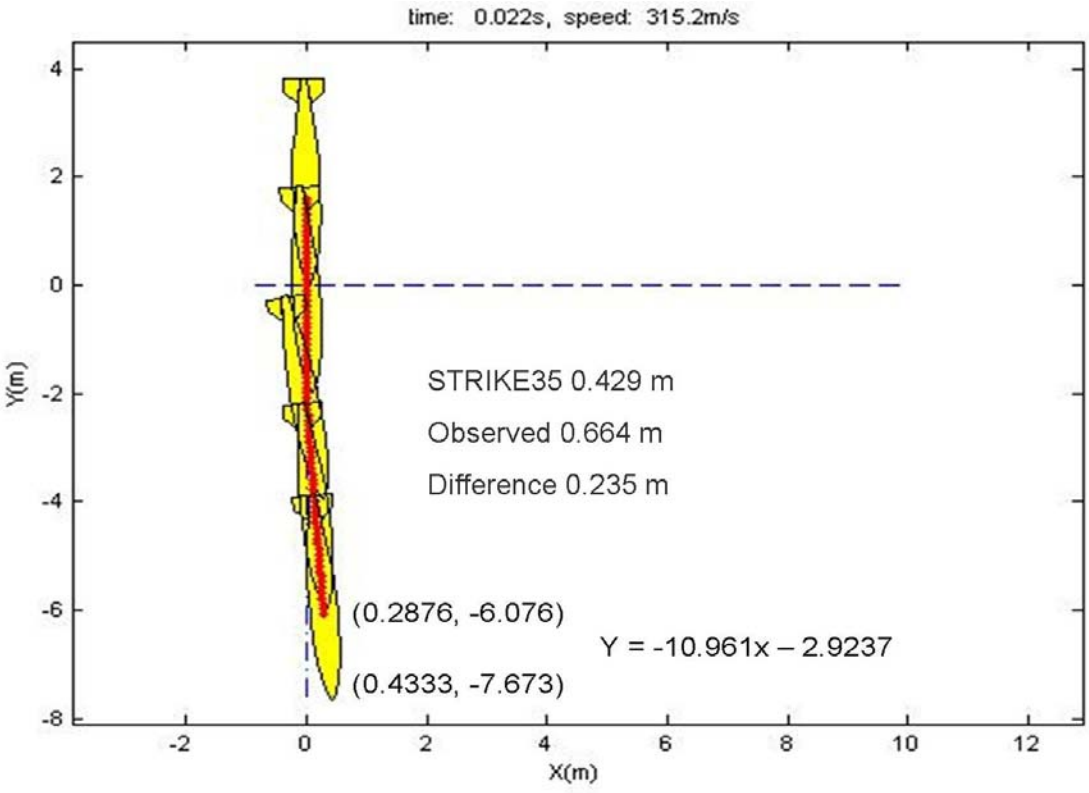

Figure 31. UTT-1(2) STRIKE35 model run with four fins

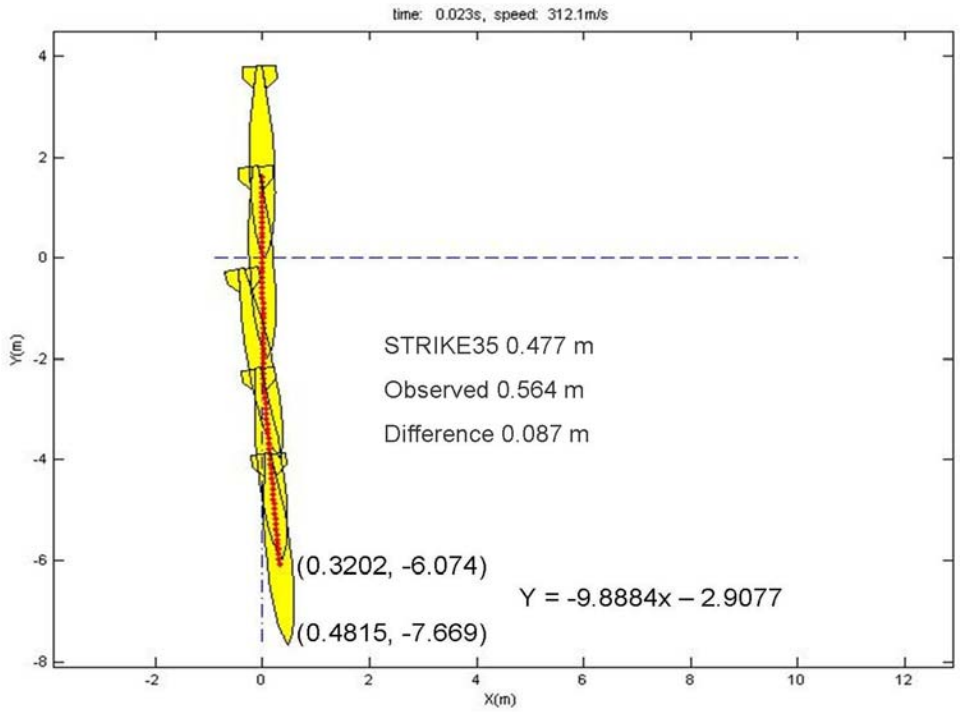

Figure 32. UTT-1(3) STRIKE35 model run with four fins

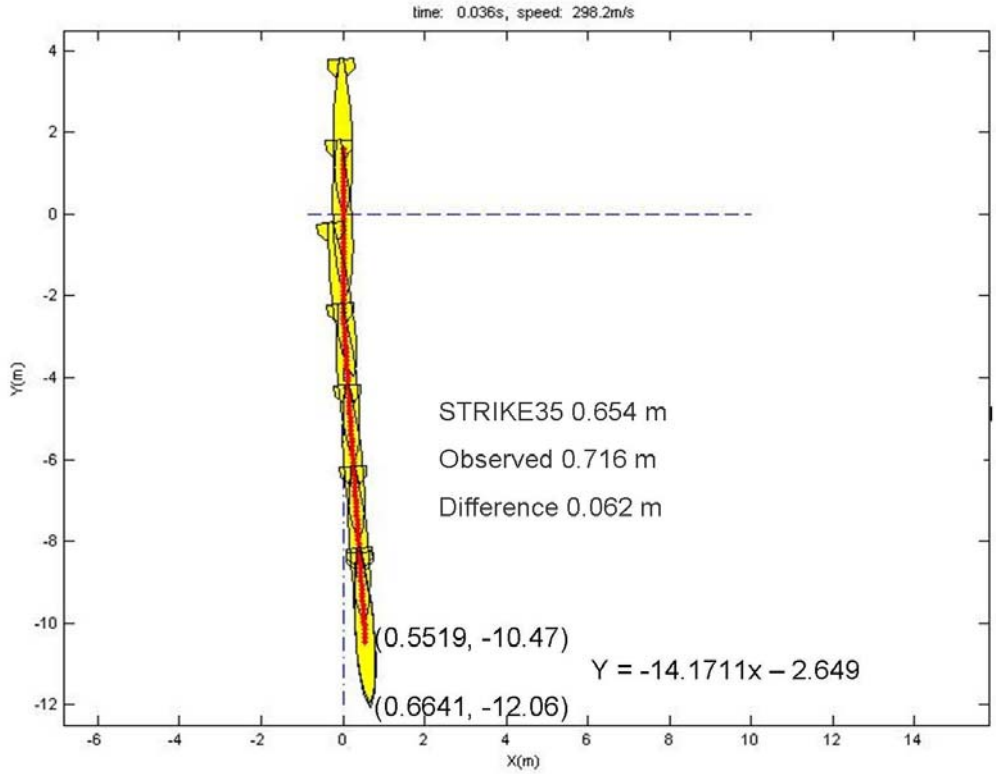

Figure 33. UTT-2(1) STRIKE35 model run with four fins

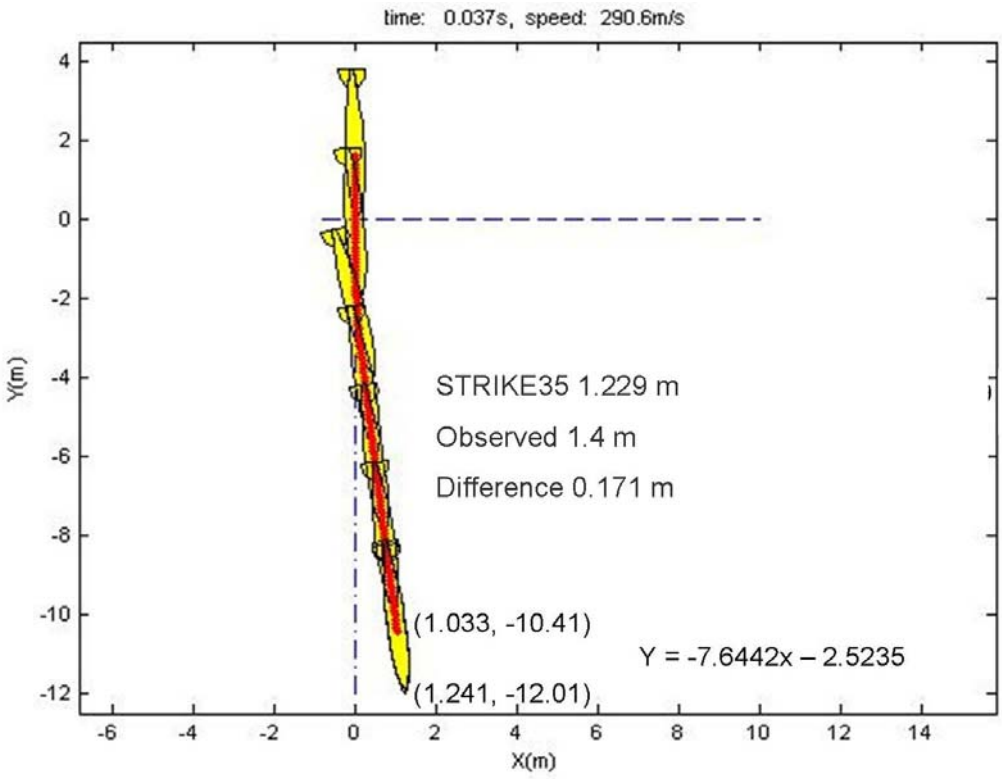

Figure 34. UTT-2(2) STRIKE35 model run with four fins

In order to use STRIKE35 to evaluate if and how many tail fins were lost in each run, we first needed to validate the model physics for the fins breaking mid-trajectory. We modified STRIKE35 (Appendix) to be able to input structural failure depth and the ability to choose either two fins or all four fins breaking off. When the model runs UTT-2(2) without tail fins due to a structural failure at water impact, Figure 35 shows the weapon tumbles around 5 m. The horizontal displacement of the model (3.8 m at 12.2 m depth) is far worse than the observed. When UTT-1(2) and UTT-1(3) are modeled with the tail departing at water entry, they show very similar tumbling; the weapon tumbles beyond horizontal at the shallow pond bottom, and the horizontal displacement of their centroids is about 1.5 m at 7.6 m depth. By analyzing many more scenarios of tail breakage, the decision was made not to allow for tail failure input into STRIKE35 at this time. The amended program also does not add the option to select tail failure due to there being little evidence in the observed data of this actually occurring mid-water column.

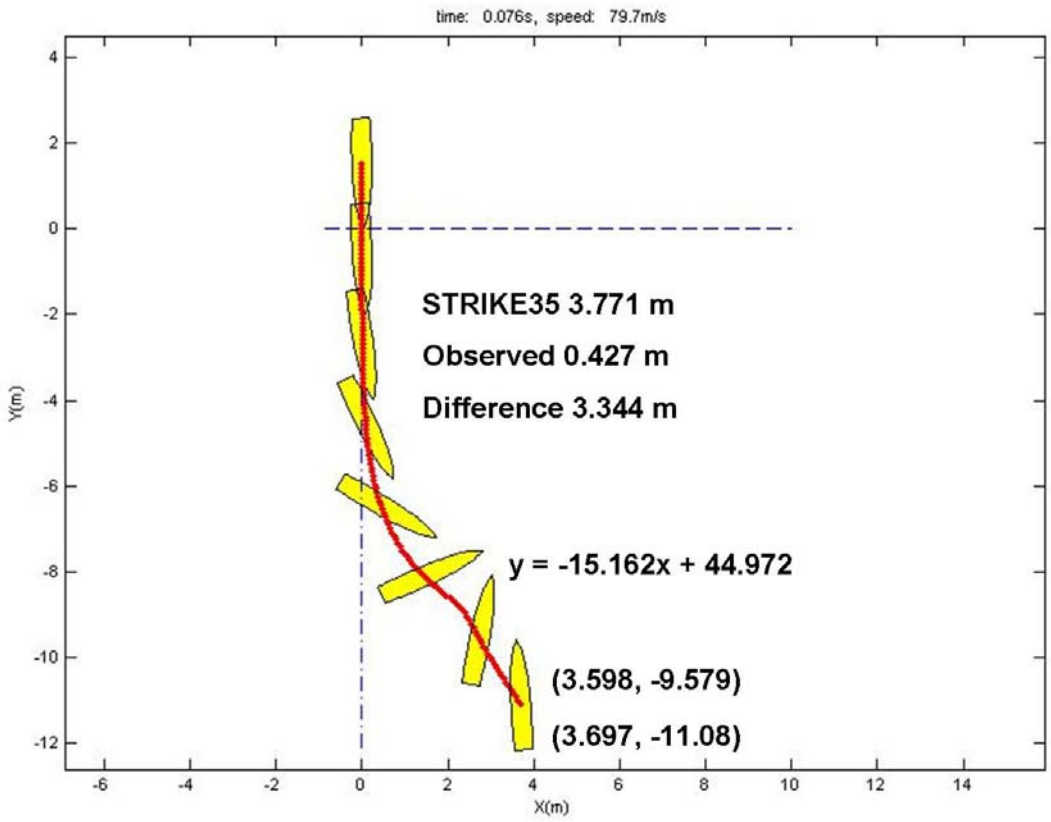

Figure 35. UTT-2(2) STRIKE35 model run for tail section breaking off at water impact

The fact that we know the depth that UTT-2(1) lost a tail fin allowed us to extrapolate the possible scenarios. Analyzing two fins and four fins breaking off when the nose reached 5.5 m depth allowed a comparison against the different structural damages, as well as an evaluation of the model against the experiment. The observed data had a displacement from the water impact point of about 0.716 m. Figure 36 shows the model's representation of two fins departing the weapon when the nose reaches 5.5 m, and the results are within 0.061 m. The more accurate model depiction had four fins breaking off and a difference in horizontal displacement of 0.005 m from water impact point (Figure 37). Both demonstrations are within the measurement error of 0.3 m.

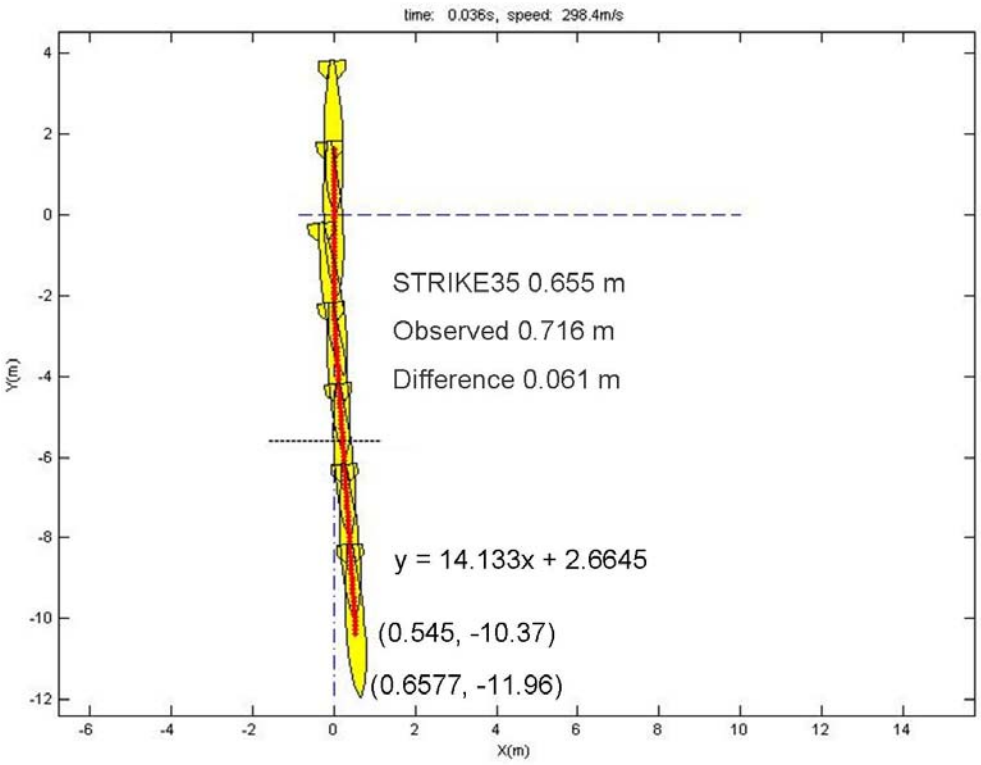

Figure 36. UTT-2(1) STRIKE35 model run for two fins all breaking off at 5.5 m

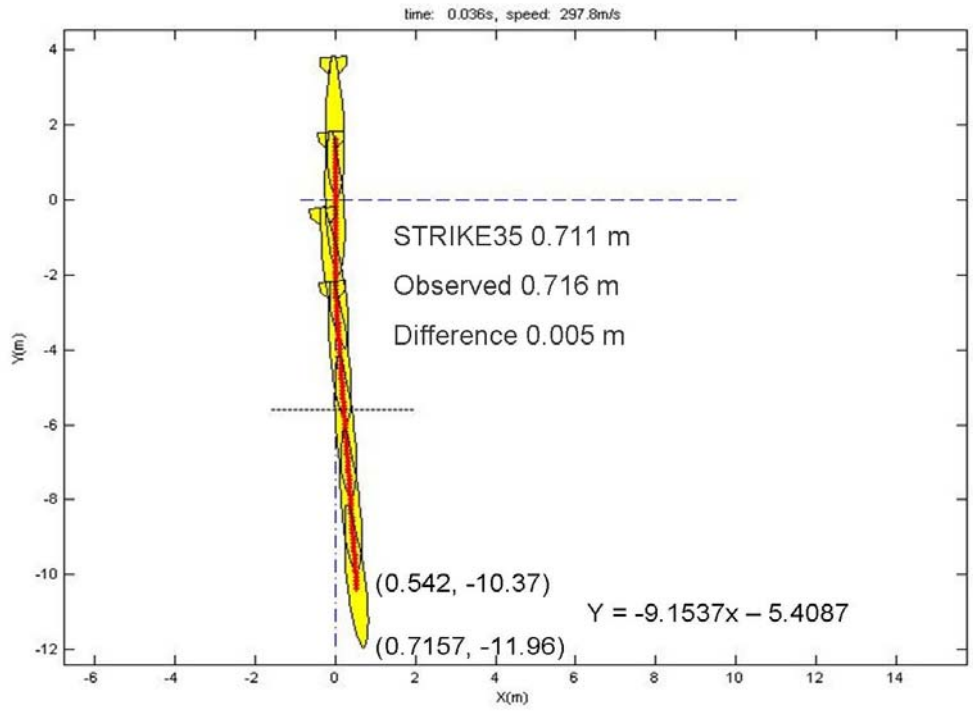

Figure 37. UTT-2(1) STRIKE35 model run for four fins all breaking off at 5.5 m

C. ASSUMPTIONS

When creating STRIKE35, they made several assumptions in order to make the model linear. When comparing the model to the observations, small errors could occur due to the following reasons: how the tail fins fall off the weapon, the shape of the nose cone, the model smoothes the body of the bomb, and the modeling location of two tail fins. When using the amended STRIKE35 version and selecting any tail fins to come off during the trajectory through the water, the fins fall off together and within a millisecond. The nose cone in JABS and the SRI experiments was the Navy Ogive type, whereas the SOABWFI Flight Testing experiments use the MXU-735 nose cone (Figure 38). Because STRIKE35 used the SRI data set in its creation, the model also uses the pointed Ogive nose cone, instead of the blunt MXU-735. The same reasoning applies to why the model does not include suspension lugs or the guidance band when creating the structural outline of the bomb (Figure 39). In order to maintain simplistic modeling features, they assumed that the weapon is an axially symmetric, rigid body; therefore, the two tail fin configuration is in the same plane instead of being perpendicular like the SRI experiment.

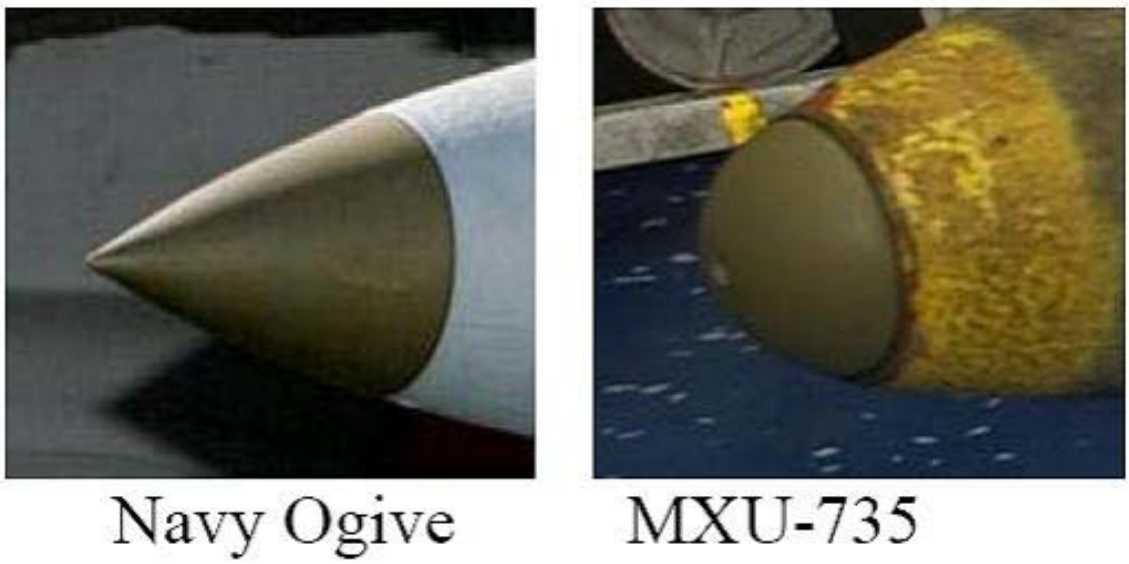

Figure 38. Ogive used for JABS, SRI and STRIKE35, whereas SOABWFI flight test used MXU-735

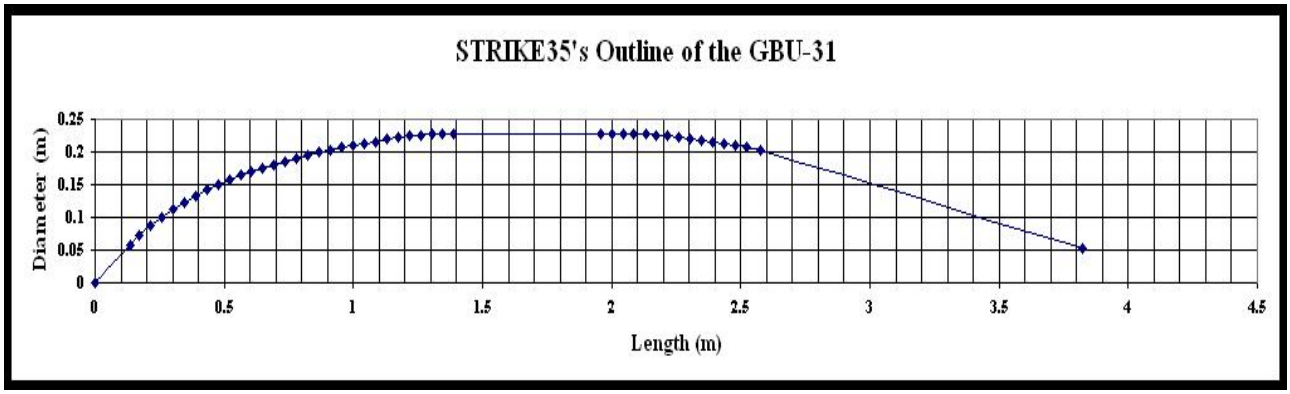

Figure 39. STRIKE35's outline of the GBU-31 body

Lastly, utilizing the maximum density of pure water, 1000 kg/m^3 at 4° C, is standard for scientific models. The UTT-1 report stated the pond's water temperature was about 35° C and the salinity near zero in the brackish pond (Boeing 2009b). This would put the density at about 996 kg/m^3 (pure water at 35° C). Of course, the density difference will change the trajectory of the weapon through the water, as density is directly proportional to the hydrodynamic forces. Comparing the same run using STRIKE35 with its current density of 1000 kg/m^3 to the observed density of 996 kg/m^3 shows little difference though (Table 5). The average density for surface seawater (in the mixed layer) is about 1027 kg/m^3. Table 5 shows that the change in density from 1000 kg/m^3 to 1027 kg/m^3 makes a bigger difference in horizontal displacement than the change from 1000 kg/m^3 to 996 kg/m^3 (0.034 meters vice 0.004 meters), but both remain within the error of measurement. One interesting fact the table shows is that an alteration in density, though linear in the hydrodynamic forces, is not linear in the trajectory (or horizontal deviation at a certain depth). Instead, it changes the way the weapon "flies" in the water, and clearly in the ocean densities, it is not a linear change.

Water Type	Density (kg/m^3)	Displacement (m)
freshwater at 95° F	996	0.414
freshwater at 4° C	1000	0.418
saltwater	1024	0.462
saltwater	1025	0.444
saltwater	1026	0.390
saltwater	1027	0.452
saltwater	1028	0.450
saltwater	1029	0.443
saltwater	1030	0.432

Table 5. Four fin GBU-31 nose displacement at 10 m depth. Water impact speed and AOA: 381 m/s and 1°

D. MODEL APPLICATION

1. Finding the Tail Breakage Depth

In the cases used to validate STRIKE35 [LFFD-1 and UTT-2(1)], the model seems to work well, within measurement error, for either four fins or two fins breaking off the weapon. The three remaining cases we have complete impact data for [UTT-1(2), UTT-1(3), and UTT-2(2)] also have evidence that fins broke off while descending to the pond's bottom, though it is unknown where and how many. For this challenge, we can use the adapted STRIKE35 for fins breaking in the water column and some logic to hypothesize how many fins and at what depth they broke. For each case, we ran STRIKE35, inputting the initial water impact characteristics, and broke off either two or all four tail fins at different depths (Table 6). Using the break-off option, two things are evident for the UTT experiments: 1) both types of breakage give results within measurement error, and 2) four fin failure shows the closest "observed to model" distances.

Experiment	Breakage Depth (m)	Model Displacement (m)	Observed to 2 Fin Failure Distance (m)	Observed to 4 Fin Failure Distance (m)
UTT-1(2)	NA	0.43	0.24	0.24
UTT-1(2)	4.6	0.44	0.24	0.23
UTT-1(2)	3.3	0.50	0.23	0.16
UTT-1(2)	2.4	0.62	0.23	0.05
UTT-1(3)	NA	0.48	0.09	0.09
UTT-1(3)	4.6	0.48	0.09	0.08
UTT-1(3)	3.3	0.56	0.09	0.01
UTT-1(3)	2.9	0.57	0.09	0.00
UTT-2(2)	NA	1.23	0.80	0.80
UTT-2(2)	4.6	1.33	0.84	0.90
UTT-2(2)	3.3	2.30	1.23	1.87

Table 6. Tail fin breakage at depth and associated displacements

With all four fins breaking off at the same time, the least amount of error in bottom horizontal displacement between the model and the observed occurred before the tail section hit the water for the UTT-1 experiment model runs. In UTT-1(2) and UTT-1(3), the nose depths were 2.4 m and 2.9 m, respectively. This is a strong indicator that the tail fins did not survive very long after impact with the water. Because the tail section does not enter the water until the nose is about 3.3 m, we have included the STRIKE35 runs where all four tail fins break when the nose reaches 3.3 m depth of UTT-1(2) and UTT-1(3) as Figures 40 and 41, respectively. The hypothesis that the fins departed not long after water impact directly contradicts the JABS trajectory analysis that showed an initial AOA less than two degrees will maintain structurally integrity beyond 28 msec;

not only did these two observations hit the water surface with less than 2° AOA, but STRIKE35 shows their trajectory to the bottom taking about 23 msec.

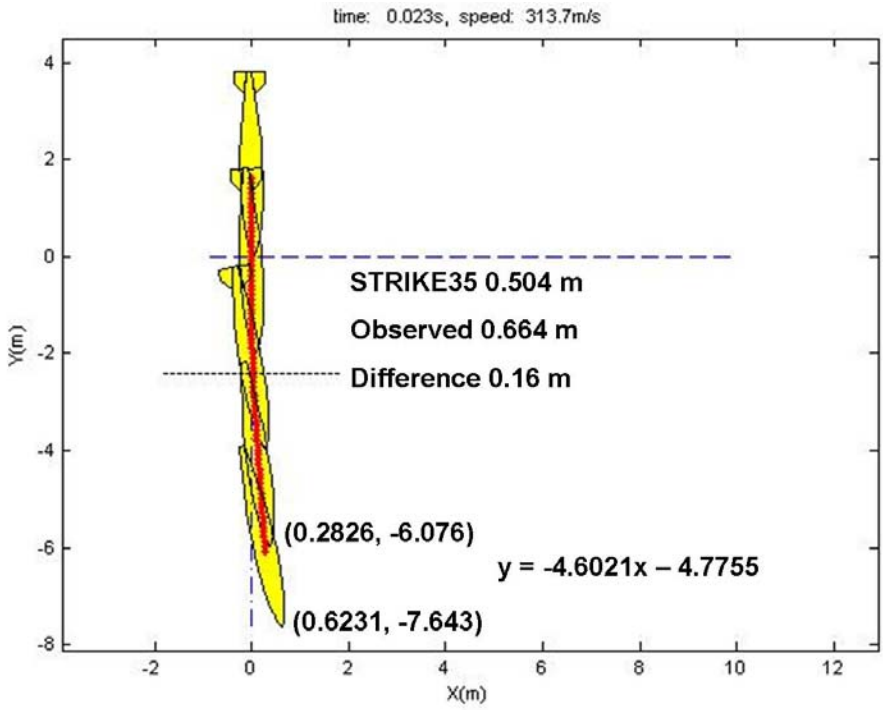

Figure 40. UTT-1(2) with all four tail fins breaking off as the nose reaches 3.3 m

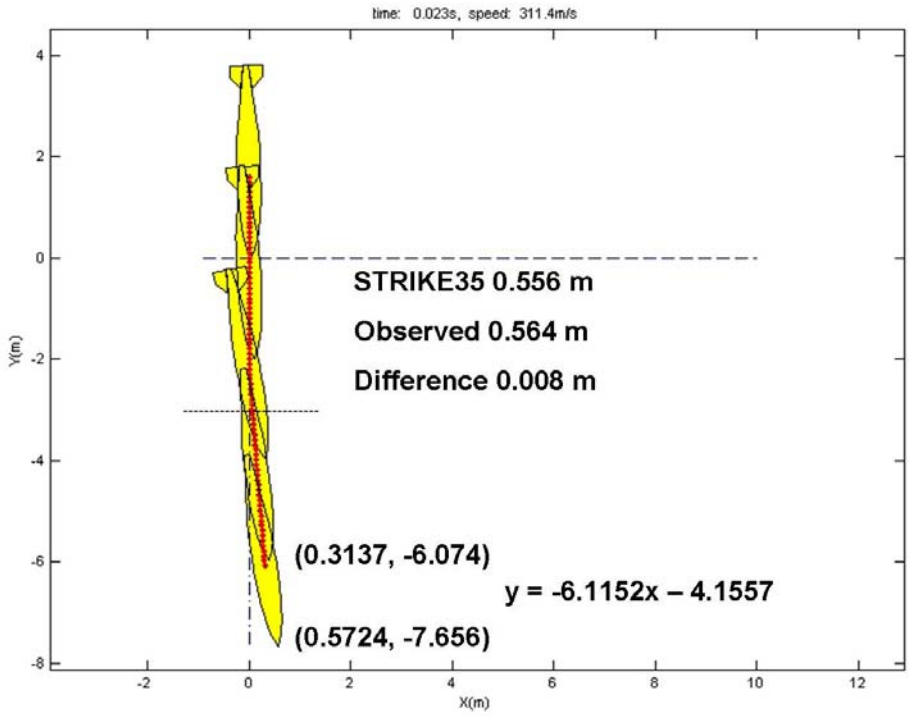

Figure 41. UTT-1(3) with all four tail fins breaking off as the nose reaches 3.3 m

UTT-2(2) was difficult to figure out using Table 4 data and the amended STRIKE35. Working backwards to find the tail breakage depth was more challenging due to the way the bomb travels in the water after a higher (greater than about 2°) water impact AOA. A difference between UTT-2 and UTT-1 is the pond depth, which one might think would give the weapon more time and even greater horizontal deviation at the pond bottom. Nevertheless, as seen in Table 6, breaking all four tail fins off at shallower depths inside the water column created continuously growing horizontal deviation. Even keeping the tail fins and breaking only two fins off did not reduce the error.

Another difference between UTT-2(2) and the previous UTT experiment is that the weapon was at a shallow enough angle when penetrating the pond bottom that is was able to tunnel. The tunneling behavior matches the SRI report claim that a bomb without tail fins has greater water trajectory curvature, as long as the weapon had enough depth to turn. Figure 42 shows that when all four tail fins break half way down the water column

(5.5 m depth in a 12.2 m pond), the bomb still does not have enough time to begin turning prior to hitting the bottom. From this, we infer that in order to get the bottom impact angle shallow enough to allow for tunneling, the bomb has to lose its tail fins closer to the surface. The SRI claim and the previous examination of UTT-1 leads to the guess that all four tail fins break off when the tail fins enter the water (when the nose reaches a depth of 3.3 m), but the error here is actually the highest (Table 6).

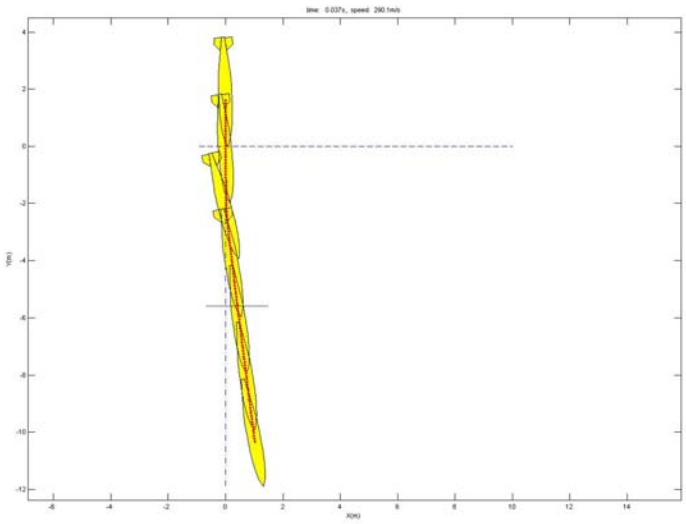

Figure 42. UTT-2(2) with all four tail fins breaking off as the nose reaches 5.5 m

After reading the previous paragraphs, it is curious how UTT-2(2) remained within 0.43 m of its water impact point. Interestingly, through a thorough examination of all initial inputs into STRIKE35 (with the density at 1000 kg/m^3), without tail fins and above an initial impact AOA of about 2°, the trajectory through the water is extremely sensitive to impact AOA. Depending on the impact AOA, either the bomb's trajectory through the water will continue smoothly in a curved path (as seen in the SRI data) or it will progress one way to a certain depth and then curve the opposing direction for the remainder of its path. The difference of 0.1° impact AOA can change the trajectory, and another 0.1° can change it back again. This turn-back trajectory can even happen at very low impact AOA (around 1°), and is affected by impact speed, as well as the density of the water.

Detecting this sensitivity allowed for a supposition about the observation to model anomaly. With the observed impact AOA interpretation being ±0.5°, it is feasible that the impact AOA for the second weapon was slightly different from what the UTT-2 report stated. If we increase the adapted STRIKE35 (with all four tail fins removed at 3.3 m) AOA input by 0.015° to 2.285°, the path of the bomb curves one direction and then turns to curve back towards the water impact point (Figure 43). This is the closest impact AOA to the UTT-2 report that results in the pitch-back trajectory, and the error is 0.70 m. Nonetheless, the closest model run to the observed initial characteristics and bottom impact point was the STRIKE35 initial AOA input increase of 0.025° to 2.295° (Figure 44). This error is 0.30 m, which is within measurement error.

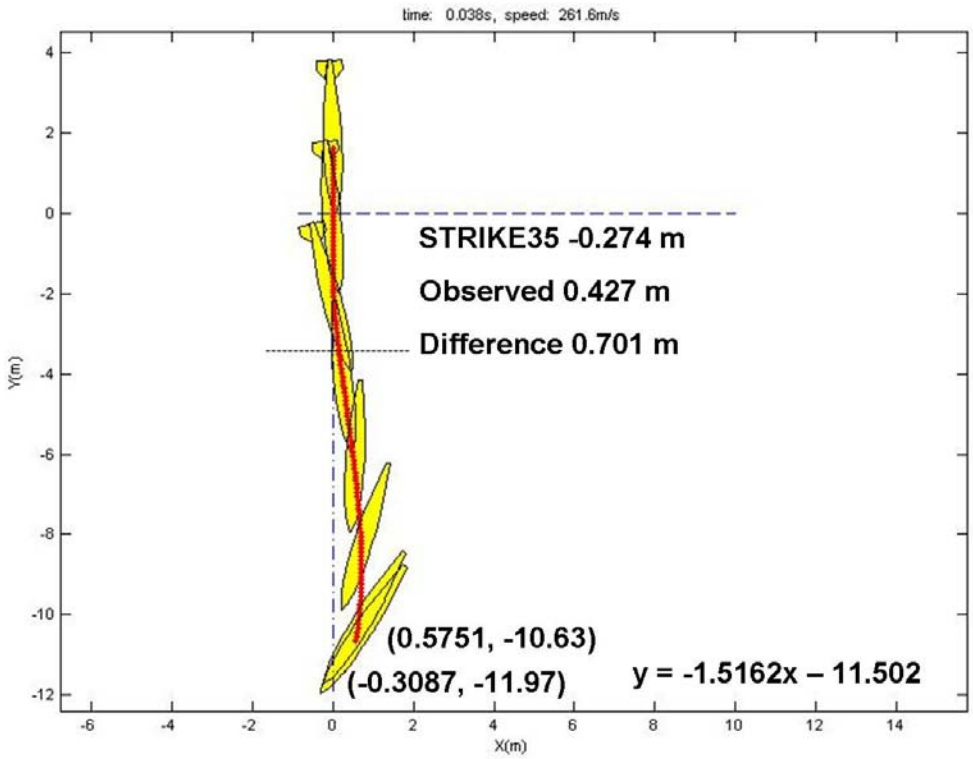

Figure 43. UTT-2(2) when AOA increased to 2.285°

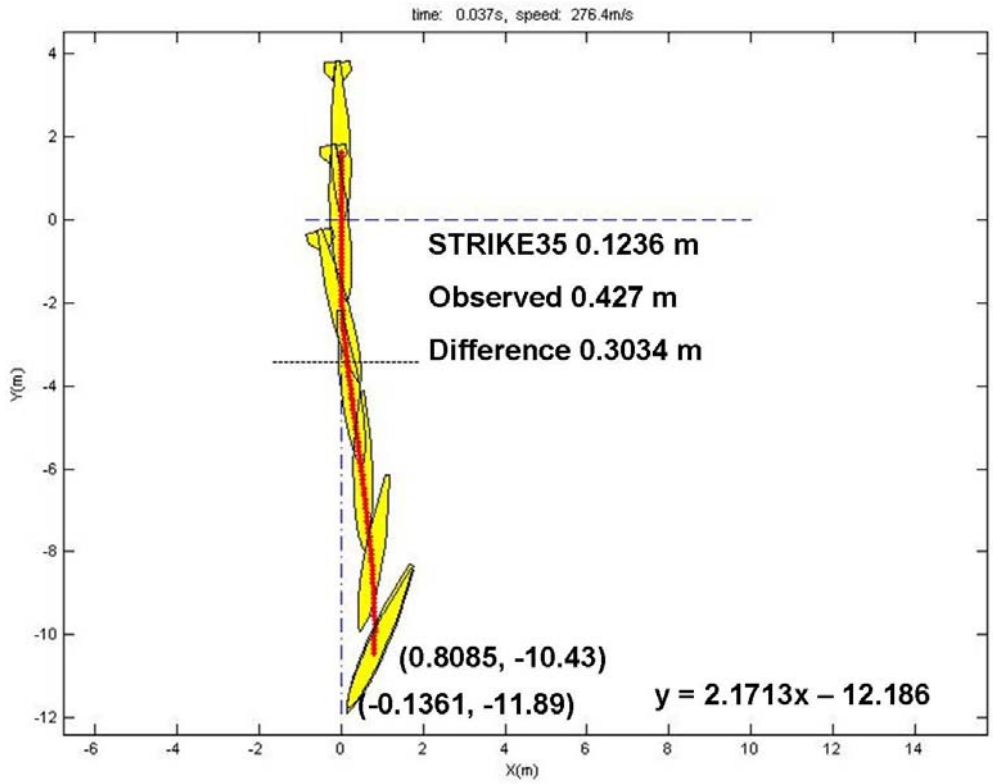

Figure 44. UTT-2(2) When AOA increased to 2.295°

2. Finding the Impact AOA Limitations

The Technology Transition Agreement (TTA) between the Office of Naval Research and the Navy states that the "trajectory deviation from the flight path angle (velocity vector) should not exceed 7 ft (2.1 m) (approximate) for water depths of 10-40 ft (3-12.2 m)" (Humes 2007). Based on these limitations, this study terminates analyzing different initial inputs when the weapon continuously exceeds 2.1 m from the water impact point. The forthcoming analysis also includes airspeeds within a reasonable window for a standard JDAM drop (381 to 396.4 m/s). Knowing that STRIKE35 correlates well with LFFD-1 and UTT-2(1), both evaluated at a standard water density of 1000 kg/m^3, we assume that the model also correlates when the density matches the environment of the observed weapon.

The first impact AOA and speed analysis is of the China Lake 12.2 m pond, with a density of 996 kg/m^3. The second analysis is a hypothetical 12.2 m ocean environment

with a density of 1027 kg/m^3. These cases are identically analyzed as the worst scenario, with all four tail fins separating from the weapon upon water entry (when the nose reaches 3.3 m) and the horizontal displacement is measured from the water impact point to the tip of the weapon's nose, not the point of the explosive. The last analysis is of the detonation position, in the same ocean environment, for each of the delay settings within the FMU-139 fuze. These settings are 0 msec (impact), 10 msec, 25 msec, and 60 msec, but this report only includes the last three. The evaluation of each delay setting will be the same worst case described above.

a. China Lake, Worst Case Analysis (Density of 996 kg/m^3)

In Figure 45, the plot shows the horizontal displacement from the water impact point (m) as a function of AOA ($^\circ$) in 35°C freshwater. Each line color represents a different water impact speed of the weapon, in increments of about 1.5 m/s. In every case, the weapon's fins immediately fall off when the nose reaches a depth of 3.3 m and the weapon travels to a depth of exactly 12.2 m. This figure pictorially explains why UTT-2(2) was such a difficult case to analyze. The weapon can take a single trajectory, like the SRI experiment (Figures 10 through 12) or the pitch back trajectory, as seen in UTT-2(2) (Figures 43 and 44).

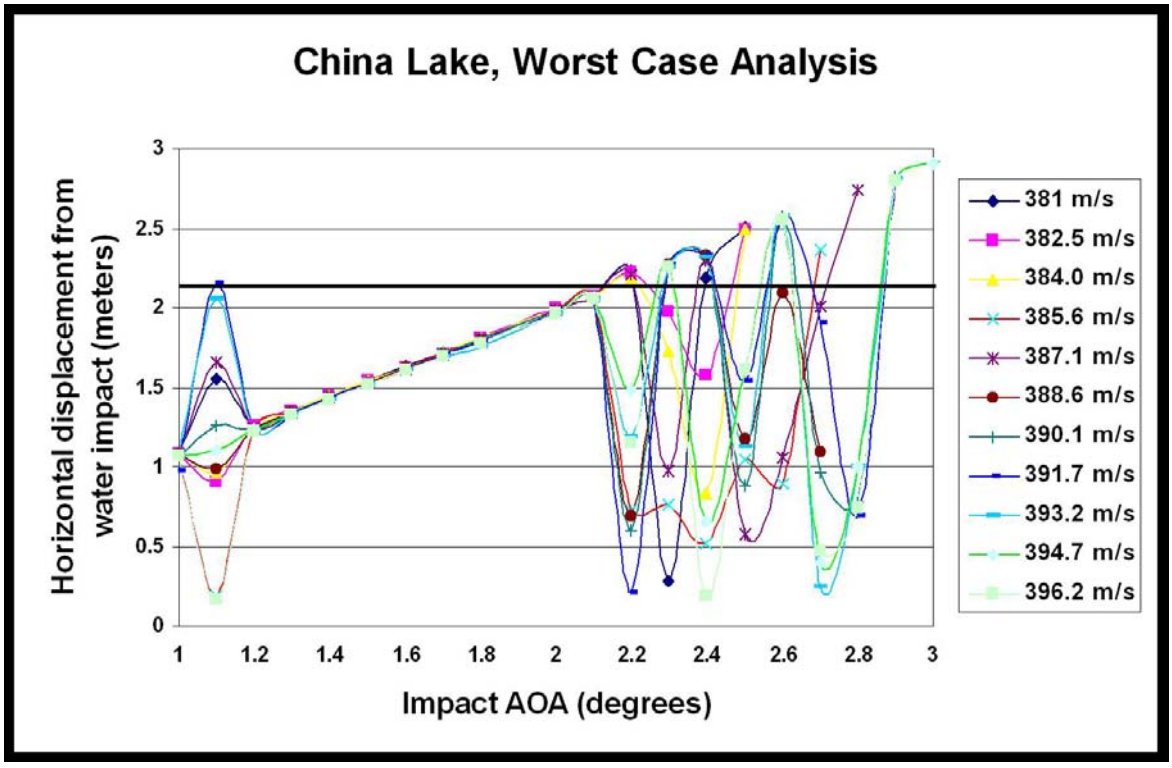

Figure 45. Weapon displacement vs. AOA in 35°C freshwater

As seen by the coincidence of most lines below an impact AOA of about 2°, the impact speed does not affect a weapon's ultimate horizontal displacement from water impact point very much. Hence, impact speed does not change the weapon's horizontal displacement as much as impact AOA does. Figure 45 also shows that when the weapon pitches back, it will not exceed the TTA until a higher impact AOA. Lastly, between about 1.2° and 2.1°, the displacements appear to increase linearly with the impact AOA (Figure 46).

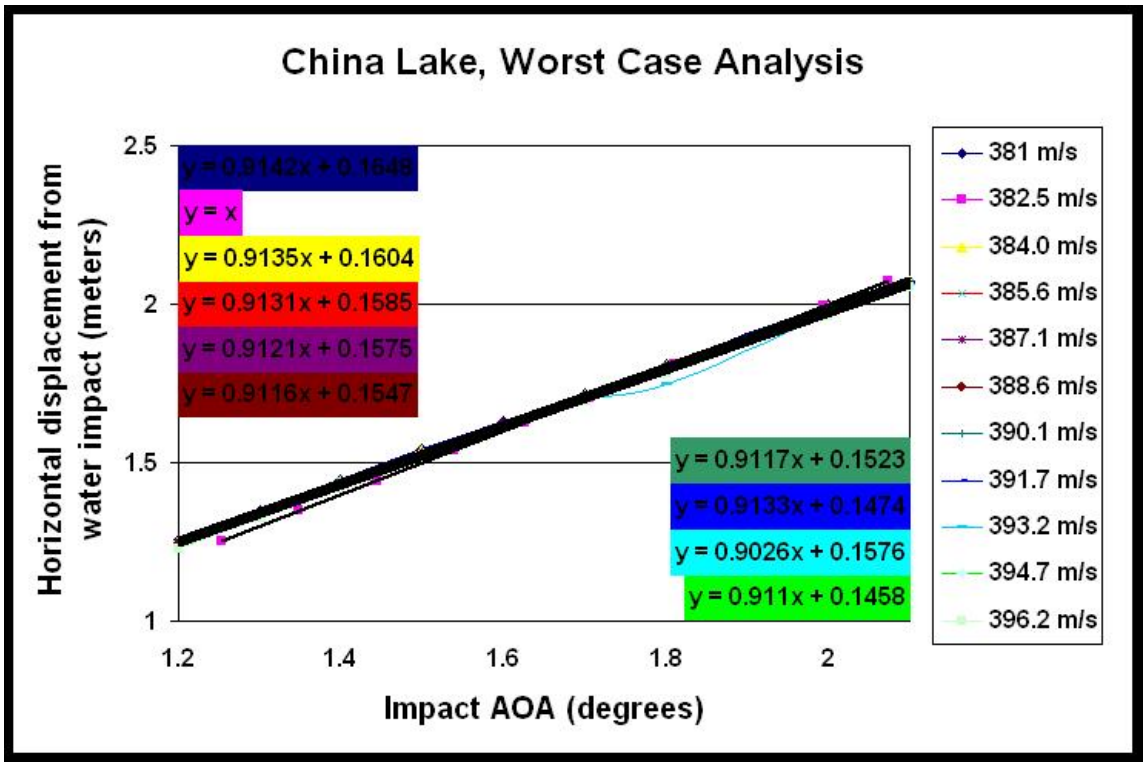

Figure 46. Most impact speeds have almost linear horizontal displacement between about 1.2° and 2.1°

All of the impact speeds remain within the TTA allowable deviation up to an impact AOA of 2.1°. At or below 384 m/s and at 387.1 m/s, the weapon continues the first type trajectory, exceeding the TTA between 2.1° and 2.2°. Between impact AOA of 2.2° and 2.4°, these impact airspeeds transition to pitch back trajectory, allowing them to stay within the TTA longer. The best case for remaining within the limits of the TTA for the greatest range of AOA is an impact airspeed of 385.6 m/s. Of course, this is right in the middle (about ±1.5 m/s) of the impact speeds with lesser AOA tolerance, but this airspeed appears to have the pitch back trajectory type until the AOA of 2.6°. The remainder of the airspeeds transition to the pitch back trajectory at 2.1°, allowing these impact speeds not to exceed the TTA limit until 2.3° impact AOA.

b. Ocean, Worst Case (Density of 1027 kg/m^3)

Figure 47 is the displacement (m) from the water impact point as a function of AOA (°) in an average mixed layer density in a hypothetical ocean. Each line

color represents a different water impact speed of the weapon, in increments of about 1.5 m/s. In each case, the weapon's fins immediately fall off when the nose reaches a depth of 3.3 m and the weapon travels to a depth of exactly 12.2 m. This figure shows that the weapon travels differently with an increase in density.

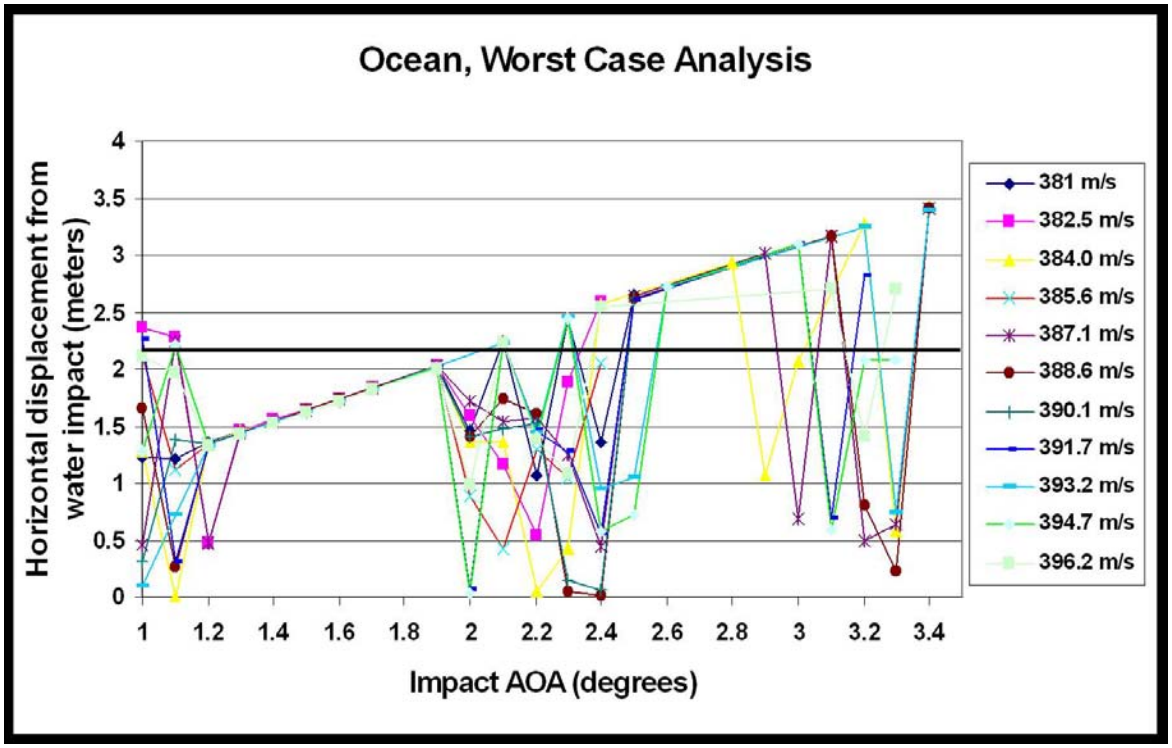

Figure 47. Weapon displacement vs. AOA in a hypothetical ocean mixed layer

Just like the lower density case, the mixed layer has the same two types of trajectories. One readily observed difference between the pond and the ocean is in the low AOAs; all airspeeds, except 381 m/s, start out traversing the water with a pitch back trajectory. Between the impact AOA of about 1.1° and 1.9°, the weapon transitions to the single curve trajectory style and remains within the TTA margins. Similar to the lower density case, above 2° all impact speeds experience flip-flop between both types of path. The best case for remaining within the limits of the TTA for the greatest range of AOA are impact airspeeds of about 387.1 to 390.1 m/s which allow an impact AOA of up to

between 2.4° and 2.5°. The upper and lower limit of our sample, 381 m and 396.2 m, both only allow up to 2.1° AOA before departing the TTA boundary, while the remaining impact airspeed allow an AOA of around 2.3°.

c. FMU-139 Fuze, Worst Case (Density of 1027 kg/m^3)

The SOABWFI Flight Tests used the 10 msec delay on the FMU-139 fuze for the 7.6 m pond demonstrations (LFFD-1 and UTT-1) and the 25 msec delay for the 12.2 m pond demonstrations (UTT-2). The last delay, not used yet in the SOABWFI program, is the 60 msec delay. This fuze also has a ± 20% tolerance that can detonate the bomb within the time limits. As in the previous examinations, the worst case means that all the tail fins break off when the nose is at 3.3 m (tail impact). During this investigation, we annotate the deviation from the water impact point as a function of time instead of depth. The model is run at each delay setting, at its lower limit (delay – 20%), and at its upper limit (delay + 20%). The horizontal displacement at the actual delay setting is the solid line, whereas the top of the error bar depicts the upper time limit's displacement and the bottom of the error bar represents the lower tolerance's deviation from water impact point. Because we are only interested in the horizontal deviation from the water impact point, the displacement at the actual delay setting is always the absolute value. Once again, the range of impact speed is from 381 to 396.4 m/s; this time in about 3 m/s increments because the previous analysis shows the weapon is not as sensitive to its initial speed.

In the ocean, the 10 ± 2 msec delay (Figure 48) remains within 1.8 m from the water impact point, no matter the impact airspeed or AOA. Similar to the findings of the SRI experiment, the greatest impact speed had the greatest deviation and the lowest impact speed had the least deviation from the water impact location for most of the impact AOAs. One observation is that the greater the impact AOA, the greater the upper (+ 20%) and lower (- 20%) variation. In addition, at lower impact AOA (below about 8°), the lower variation is much larger than the upper variation.

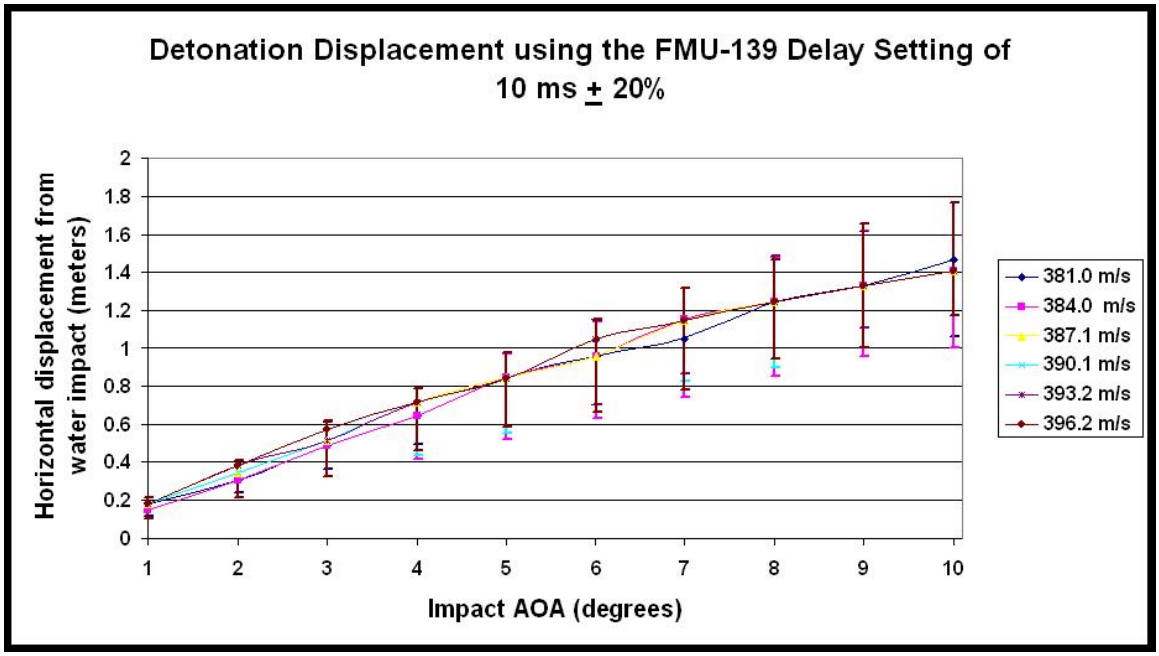

Figure 48. Weapon displacement vs. AOA for 10 msec ± 20% delay

The 25 ± 5 msec delay (Figure 49) remains within 2.1 m from the DPI, no matter the observed airspeed, up to an impact AOA of about 4°. Though the lowest impact speed (381 m/s) has a greater deviation from DPI below 3°, the highest speed (396.2 m/s) always has the greatest variation and has the highest deviation from 3° on. Opposite the shorter delay setting, this time the upper variation (+ 20%) seems to effect the deviation from DPI more so than the lower (- 20%). One observation is that the lower limit and the delay setting are always within the TTA, but it is the upper limit that reduces the available impact AOA.

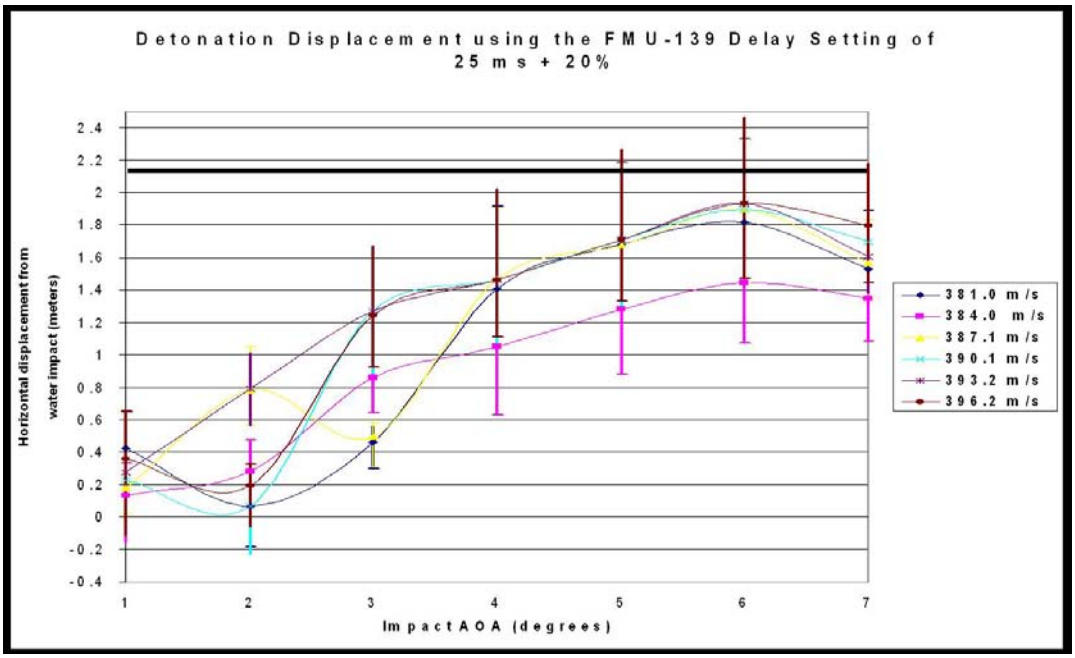

Figure 49. Weapon displacement vs. AOA for 25 msec ± 20% delay

The 60 ± 15 msec delay (Figure 50) is not part of the TTA, but the availability of the setting makes it an interesting case study. All of the impact airspeeds and AOA up to 3° remain within about 8 m of the water impact point. One observation is that the higher impact speeds, 390.1 to 396.2 m/s, have the greatest variation in their tolerances. Allowing the user to choose less than 3° impact AOA and below 390.1 m/s impact speed, would reduce the horizontal deviation to 7 m.

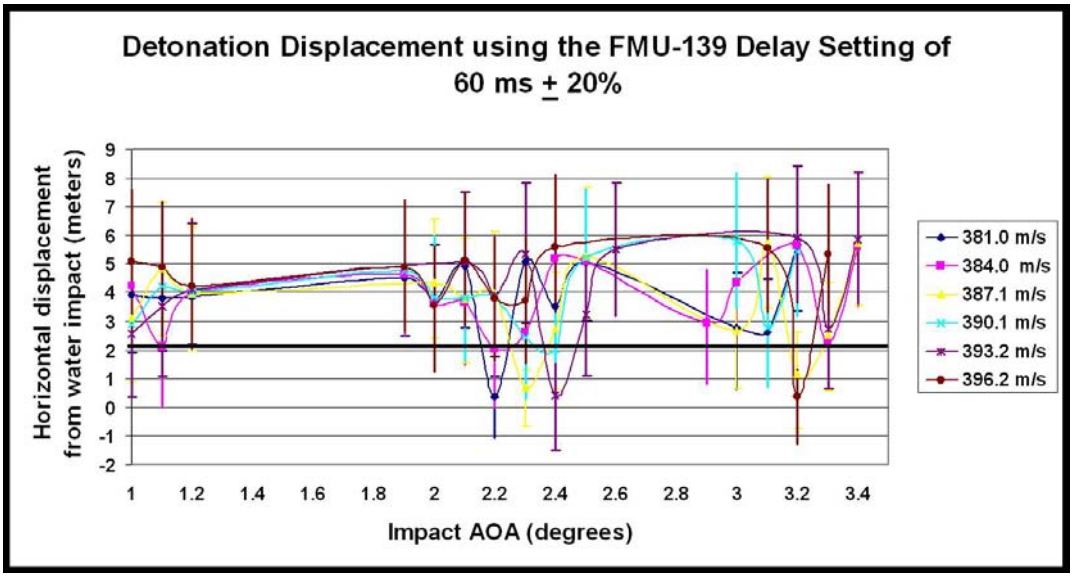

Figure 50. Weapon displacement vs. AOA for 60 msec ± 20% delay

V. DISCUSSION

A. STRIKE35 UTILITY

All of the live and inert weapons launched into the pond at China Lake provide the proof of concept for the JABS as an organic mine neutralizer. The weapon maintains stability in the water column and remains within 2.1 m of the water impact point. STRIKE35 is useful to the proof of concept in that, with known start and end-points, it describes the path of the weapon through the water. The model can clarify if and where the weapon lost its tail section or tail fins. It is also valuable in validating other methods of data collection.

In this analysis, STRIKE35 identified, using the impact points for the water and pond bottom, that it is probable the UTT tail fins did not remain intact long after submersion. Using it to investigate UTT-2(2) also shed light on the sensitivity to impact AOA, and the lack of sensitivity to impact speed of the weapon, on the overall horizontal deviation from water impact point. No matter the speed, about 2.1° is the cutoff impact AOA for predicting how the bomb will travel in the pond. Beyond this AOA, the weapon could continue to travel in a simple curve or could transition to a more complex, pitch back curve. The ability to predict which path the weapon will take becomes almost impossible, as a change as small as 0.015° impact AOA can transition the weapon from one path to the other.

The model also shows that density affects the type of trajectory, especially around 1° AOA, but does not affect the magnitude of the horizontal deviation from water impact. This is useful when applying the lessons learned about the weapon in the pond to the operational environment. Using a hypothetical ocean mixed layer density, STRIKE35 then solved for the limitations on impact speed and AOA of the weapon for the FMU-139 fuze delay settings. We found the 10 mecs delay is unlimited between 381 and 396.4 m/s impact speed, as well as beyond a 10° impact AOA. The 25 msec delay, for the same speeds, is limited to below a 4° impact AOA, and the 60 msec delay is currently not useful (under the TTA restrictions).

B. FUTURE USES AND RESEARCH

Once the TTA is accepted, STRIKE35 can assist choosing the parameters for a correct launch acceptability region (LAR) when planning the AMCM mission. The LAR is a region where a launched weapon can successfully reach the target. Because the JDAM is a glide weapon, the kinematic performance (energy of the weapon during flight) is the limiting factor in defining the LAR. By selecting the impact of the water as vertical (90°), the LAR shrinks to the point of only being able to drop a few weapons. Using STRIKE35, we observed the impact AOA could be less than vertical and remain within the TTA limitations.

STRIKE35 showed the limitations of the 60 msec delay fuze setting for this weapon and the TTA. SRI is currently looking at flatter nose cone shapes that create a larger cavity, allowing the weapon to travel straight for a longer distance. If their experiments prove the concept, another amendment to STRIKE35 could be useful in evaluating the new nose cone on the weapon.

Some areas not looked at in this analysis includes the structural integrity of the entire tail section, as well as wave effects on the weapon's horizontal deviation and structural integrity. According to Boeing, the connector bolt on the tail assembly is weaker than the fin attachment bolts, but these three experiments were not affected by this fragile area.

VI. CONCLUSIONS

According to ADM Roughead's *CNO Guidance for 2007–2008*, "Adversaries are unlikely to attempt conventional force-on-force conflict, and to the extent that maritime forces could be openly challenged, their plans will almost certainly rely on asymmetric attack and surprise." We have seen this in Iraq and Afghanistan with the improvised explosive device threat. In this same regard, the CNO has made the mine threat a top priority in his tenure. The reasons are clear: to be able to accomplish an amphibious landing, keep sea lines of communication and commerce open, deny the threat to a port disrupted by a mine laying campaign, and maintain freedom of maneuver and freedom of access.

Organic mine warfare is the newest form of mine warfare. In order to bridge the gap between the aging AMCM and the latest technology, a TTA took place to allow for the use of the GBU-31 as a mine neutralizer. Resources are in high demand and short supply to be able to test all possible scenarios, so the STRIKE35 model can assist with the final stages of the TTA.

This thesis validates STRIKE35, which is based on the $1/12^{th}$ scale replica of the MK-84, for the GBU-31. After validation, an amendment to the model allowed us to work backwards to find the depth where the tail fins broke off for three other weapons. One of the trajectories showed the sensitivity that the JDAM has to impact AOA. The AOA limitations found for a 12.2 m freshwater pond, as well as a hypothetical ocean (with the density 1027 kg/m^3) of the same depth, were below 2.1°. We found the impact speed and water density to have little bearing on the overall horizontal trajectory of the weapon from the water impact point. Finally, we observed specific fuze settings and their tolerances in the ocean environment, finding the 10 msec fuze to have no limitations and the 25 msec to be limited below 4°.

THIS PAGE INTENTIONALLY LEFT BLANK

LIST OF REFERENCES

Almquist B. Assault breaching system technologies. In: East Coast Amphibious and Mine Countermeasure Workshop; 2008 Sep 9-10; Panama City, FL. Arlington (VA): Office of Naval Research; 2008.

Almquist B, McLaughlin T. Assault breaching system technologies. In: 99th Annual Science and Engineering Annual Technology Conference/DoD Tech Exposition; 2008 Apr 15-17; Charleston, SC. Arlington (VA): Office of Naval Research; 2008.

Boeing. Stand-off assault breaching weapon fuze improvement (SOABWFI) live fire flight demonstration -1 (LFFD-1). Report No. 09J0078. 2009a.

Boeing. Stand-off assault breaching weapon fuze improvement (SOABWFI) underwater trajectory test - 1 (UTT-1). Report No. 09J0059. 2009b.

Boeing. Stand-off assault breaching weapon fuze improvement (SOABWFI) underwater trajectory test - 2 (UTT-2). Report No. 09J0142. 2009c

Brown L. Mine countermeasures an amphibious operations: a line in the sea? Newport (RI): Naval War College; 1991.

Bruhn D. Wooden ships and iron men: the U.S. Navy's ocean minesweepers, 1953-1994. Westminster (MD): Heritage Books, Inc.; 2007.

Conway J, Roughead G, Allen T. A cooperative strategy for 21st century seapower. Report. Washington (DC): U.S. Government Printing Office; 2007.

Chu P, Fan C, Gefken P. Diagnostic-photographic determination of drag/lift/torque coefficients of a high speed rigid body in a water column. Journal of Applied Mechanics. 2010:76:15.

Chu P, Fan C, Gefken P. Underwater bomb trajectory prediction for stand-off assault (mine/IED) breaching weapon fuse improvement (SOABWFI). Report. Monterey (CA): 2008.

Federation of American Scientists. Logistics cost factors per flying hour constant FY97 dollars [internet]. Washington (DC): c1997. [cited 2009 Sept 14]; Available from http://www.fas.org/man/dod-101/usaf/docs/hourcons.htm

Federation of American Scientists. Mine warfare overview [internet]. Washington (DC): c2008. [cited 2009 Aug 26]; Available from: http://www.fas.org/programs/ssp/ man/uswpns/navy/ minewarfare/mine_ warfare.html

Gasperini W. Uncle Sam's Dolphins. Smithsonian Magazine [internet]. 2003 Sept [cited 2009 Aug 25]. Available from: http://www.smithsonianmag.com/ science-nature/ Uncle_Sams_Dolphins.html

Gefken P. Evaluation of precision-guided bomb trajectory through water using scale-model experiments. SRI Final Technical Report. Menlo Park (CA). PYU-16600, 2006.

Hall P. We'd have to sink ships: impact studies and the 2002 west coast port lockout. Economic Development Quarterly. 2004:18(4):354–367.

Hartmann G, Truver S. Weapons that wait: mine warfare in the U.S. Navy. Annapolis (MD): Naval Institute Press; 1991.

Hines J. Sea Shield/Mine Warfare Sea Trial Lessons Learned and Future Trials [conference presentation on the internet]. In: MINWARA Spring 2005 Regional Conference [internet]; 2005 May 23-26; Panama City, FL. San Diego (CA): COMTHRDFLT; 2006 May [cited 2009 Aug 25]. Available from: http://www.minwara. org/Meetings/2005_05/Spring_2005_Agenda.htm

Humes G. Technology transition agreement EC SHD-FYO6-03 FNC Product: Standoff Assault Breaching Weapon Fuze Improvement. 2007.

Military Sealift Command [Internet]. Fast Sealift Ship Fact Sheet. Washington (DC). 2003 Dec [cited 2009 Sep 2]. Available from: http://www.msc.navy.mil/factsheet/ fss.htm

NAVAIR. JDAM/LJDAM USN/USMC Configurations. 2009.

Naval Air Weapons Center, Weapons Division. GBU-31, GBU-32 AND GBU-35 Joint Direct Attack Munitions (JDAM) tactical manual and users guide draft for USN series aircraft F/A-16C/D: China Lake (CA); 2002.

Naval Studies Board National Research Council. Committee for mine warfare assessment naval mine warfare: operational and technical challenges for naval forces. Washington (DC): National Academy Press; 2001.

Naval War College. Mine Warfare chg 1 [class presentation using PowerPoint slides]. In: Joint Maritime Operations I; 2009a Aug 28; Monterey, CA. Newport (RI): Certificate in Joint Military Education at the Naval Post Graduate School. p. 227-262.

Naval War College. Operational and Maritime Logistics 08-09 [class presentation using PowerPoint slides]. In: Joint Maritime Operations I; 2009b Sep 15; Monterey, CA. Newport (RI): Certificate in Joint Military Education at the Naval Post Graduate School. p. 14-61.

Naval War College. USAF Capabilities 08-09 [class presentation using PowerPoint slides]. In: Joint Maritime Operations I; 2009c Sep 2; Monterey, CA. Newport (RI): Certificate in Joint Military Education at the Naval Post Graduate School. p. 20-70.

Ray G. Bomb strike experiment for mine clearance operations [master's thesis]. Naval Postgraduate School; 2006 Mar 6.

Roughead G. CNO guidance for 2007-2008. Washington (DC). 2007.

United States General Accounting Office (US). Improved littoral war-fighting capabilities needed. Report to the Chairman and Ranking Minority Member, Subcommittee on Military Research and Development, Committee on Armed Services, House of Representatives. Washington (DC). U.S. Government Printing Office. 2001 May [cited 2009 Sep 3]. GAO-01-493. Available from: http://www.gao.gov/cgi-bin/getrpt?GAO-01-493

USS Ardent [internet]. [cited 2009 Sep 23]. Available from: http://www.ardent.navy.mil/default.aspx

Wardlaw A, Goeller J, Ruben K, Musho T. Underwater trajectory and stress analysis. Report. ATR FP-053. 2008.

Watson K, Makarsky J, Powell M, Goeller J. Flight test to determine underwater stability of a precision guided weapon for use in mine clearance. In: 11th Joint Classified Bombs/Warheads & Ballistics Symposium; 2009 Aug 3-6; Monterey, CA. 15. ().

Zolton, M. Warships 'find' mines that should have been cleared. Navy Times 1991 Feb 4; 40:34-35.

THIS PAGE INTENTIONALLY LEFT BLANK

APPENDIX

runMK3Dtailbreak.m

```
% this program has changed STRIKE35 to show what happens when the tail fins
% break off inside the water column, after water entry.
% Created by Chenwu Fan
global g rw m mw mwfl J L Lc d nu area yi areai voli vcyi cmr CGy yyy Re0 nfin
% set up constants
dist=0.1;     % the distance for each step
ipt=round(2/dist);% how often to plot figure of bomb
r2d=180/pi; g=9.806; % radians to degrees; gravity;
f2m=.3048; % foot to meter or ft/sec to m/s
nu=1.13e-6; ftsz=8; % dynamatic viscocity; font size
rw=1000;            % density of water
mfl=6.2425*0.454; volfl=mfl/2200;% mass of fin (kg); volume of the fin
figure('units','inches','position',[2,2,8,6]);% opening figure
% character array (no tail, no fins, 2 fins, 4 fins)
%  Assume Original Configuration is 4;
tt=input('Enter Water Depth (ft), Fin Break-Off Depth (ft), MK84 Break-Off Configuration fins: (0,2), Speed (ft/sec), Impact Angle of
Attack (degrees)  ','s');
while(~isempty(tt))% as long as character array input, this loop will run, else it exits program
   nfin=4; b=0;    % tail not broken
   clf;% clears current figure
   tt=str2num(tt);% converts a character array of numbers to a numeric matrix
   dep=tt(1); finbreak=tt(2);  bnfin=tt(3); vs0=tt(4); EL0d=tt(5); % assigns names to inputs
   dep=-1*dep*f2m; finbreak=-1*finbreak*f2m; vs0=vs0*f2m; EL0=EL0d/r2d; % unit conversion from english to metric
   n=1;
   load MK84tailsize.dat;% outline of bomb shape
   yi=MK84tailsize(:,1); ri=MK84tailsize(:,2);% length from nose to tail; radius at respective points
   L=150.51*0.0254; % length converted to cm
```

```
m=2076.64*0.454; CGy=63.12*0.0254;% mass converted to kg; center of gravity converted to cm
%%%%%%%%%%%%%%%%%%%%%%%%%%%%%
[voli,areai,vcyi,Jy,Jz,cmd,cvd,yi,ri,yoi,cmr]=getbombphysics(yi,ri,CGy,m);% program for how the bomb travels through the water
vol=voli(end); mw=rw*vol; d=2*sqrt(vol/L/pi);% renames total volume; mw=water mass=density*volume; diameter of cylinder of equal volume
J = Jz; area=areai(end);% renaming inertia and total area
m=m+nfin*mfl; mwfl=nfin*volfl*rw; mw=mw+mwfl; % if fins then add the mass and volume to bomb, and mass of water displaced
LH=yoi(1); % first y variable based on mass center and head forward
LT=L-LH; Lc=vcyi(end)-cmd;% length minus previous; volume center locations along the bomb-center of mass
% finding points for tail dimensions
y1=yoi(end)+0.75*0.0254; y2=y1; y3=yoi(end)+(0.75+9.44)*0.0254;% distance from head converted to cm
r1=interp1(yoi(end-1:end),ri(end-1:end),y1);% finds the radius at the end point
r2=25.31/2*0.0254; r3=r2;% converts the radius to cm
yy=yoi(end-1:end); rr=ri(end-1:end);%defines the current last two points
dy=diff(yy); dr=diff(rr);%find the slope between current last two points
y4=(dr*yy(1)+dy*(y3+r3-rr(1)))/(dy+dr);% defines a new last point
r4=y3+r3-y4;  % defines a new last radius
yyy=(y1+y2+y3+y4)/4;% average
yfil=[y1,y2,y3,y4,yoi(end)]; rfil=[r1,r2,r3,r4,ri(end)];%fills in the length and radii
yyi=[yoi,yfil,fliplr([yoi,yfil])]; rri=[ri,rfil,-fliplr([ri,rfil])];%creates bottom outline of the bomb
%%%%%%%%%%%%%%%%%%%%%%%%%%%%%
axes('position',[0.1,0.1,0.85,0.85],'ylim',[dep-0.5,4.5],'box','on','fontsize',ftsz);% set plot characteristics
hold on; axis('equal');
plot([-1,10],[0,0],'b--');
plot([0,0],[dep,0],'-.');
ylabel('Y(m)'); xlabel('X(m)');
clear XYZC EL AG VS;% clears center coordinate, lift direction, angle of velocity, bomb speed
OMG0=zeros(1,3);  % zeros placeholder
psiv=pi/2; psib=pi/2;%bomb velocity and bomb position azimuth angles set to 90 degrees
EL(1)=EL0-pi/2;% rotates bomb position elevation angle 90 degrees
```

```
VS(1)=vs0; AG(1)=-pi/2;% initial bomb speed and bomb velocity elevation angle
XYZC(:,1)=[0;0;CGy];% replacing first column of center coordinate matrix
[myi,mri]=rotobj(yyi,rri,EL(n));% the object (yyi,rri) rotation arf (radiau) around (0,0)
hh2=patch(XYZC(2,n)+myi,XYZC(3,n)+mri,'y'); % colors the bomb yellow
plot(XYZC(2,n),XYZC(3,n),'r.');% plots the center of mass in red
Lw=0; time(n)=0; ELAG=0;% initial
omg3D=[1e-10;0;0]; kwet=0; % initial bomb rotation velocity; kwet
while(XYZC(3,n)+min(mri)>dep & (kwet==0 | XYZC(3,n)+max(mri)<0))%while the bomb has not reached depth
   dt=min(1,dist/(VS(n)+eps));%time step
   n1=n; n=n+1; time=time+dt;%initial time
   [VS(n),AG(n),EL(n),XYZC(:,n),omg3D,psiv,psib]=bomb1step3D(dt,VS(n1),AG(n1),EL(n1),XYZC(:,n1),omg3D,psiv,psib);
   [myi,mri]=rotobj(yyi,rri,EL(n));% the object (yyi,rri) rotation arf (radiau) around (0,0)
   if(psib<0), myi=-myi; end% if bomb position azimuth angle negative then places bomb on other side
   if(XYZC(3,n)<-2.5), kwet=1; end% if depth less then -2.5 then wet
   if(ipt*floor((n1-1)/ipt)~=n1-1), set(hh2,'visible','off'); end
   hh2=patch(XYZC(2,n)+myi,XYZC(3,n)+mri,'y');% colors the bomb yellow
   plot(XYZC(2,n),XYZC(3,n),'r.');% plots the center of mass in red
   title(['time: ',sprintf('%7.3f',time(end)),'s,  speed: ',sprintf('%6.1f',VS(n)),'m/s']);
   drawnow;
   if(b==0 & XYZC(3,n)<=finbreak)
      b=1; nfin=bnfin;
      text(XYZC(2,n),XYZC(3,n),'-------------------------','color','k','horizontalalignment','center');
      if(nfin==0)% no fins
         m=2051.67*0.454; CGy=62.11*0.0254;% mass converted to kg; center of gravity converted to cm
      elseif(nfin==2)% two fins
         m=2064.15*0.454; CGy=62.60*0.0254;% mass converted to kg; center of gravity converted to cm
%       elseif(nfin==4)% four fins
%          m=2076.64*0.454; CGy=63.12*0.0254;% mass converted to kg; center of gravity converted to cm
      end
      m=m+nfin*mfl; mwfl=nfin*volfl*rw; mw=mw+mwfl; % if fins then add the mass and volume to bomb, and mass of water
displaced
```

```
        if(nfin==0)
           yyi=[yoi,fliplr(yoi)]; rri=[ri,-fliplr(ri)];% update bomb shape
        end
      end;
   end
   tt=input('Enter Water Depth (ft), Fin Break-Off Depth (ft), MK84 Break-Off Configuration fins: (0,2), Speed (ft/sec), Impact Angle
of Attack (degrees)  ','s');
end
```

```
function [ee,ev,ealpha,el,ed,evgama,evpsi]=setunitvector(gama,beta,psiv,psib);
% function [ee,ev,ealpha,el,ed,evgama,evpsi]=setunitvector(gama,beta,psiv,psib);
%         is used calculate unit vector
% input:
%   gama: bomb velocity elevation angle.
%   beta: bomb position elevation angle.
%   psiv: bomb velocity azimuth angle
%   psib: bomb position azimuth angle
% output:
%   ee: bomb axis direction vector
%   ev: bomb velocity direction vector
%   ealpha: attach angle (Hydro torque) direction vector
%   el: lift force direction vector
%   ed: drag force direction vector
%   evgama, evpsi: d(ev)/dt two compound vector.
%
%  Chenwu Fan,  NOAP,  NPS
ee=[cos(beta).*cos(psib); cos(beta).*sin(psib); sin(beta)];     % bomb direction
ev=[cos(gama).*cos(psiv); cos(gama).*sin(psiv); sin(gama)];     % velocity direction
ealpha=cross(ev,ee);
ealpha=ealpha./(sqrt(sum(ealpha.^2))+eps);                    % torque direction
el=cross(ealpha,ev);                                    % lift direction
ed=-ev;                                              % drag direction
```

```
evgama=[-sin(gama).*cos(psiv);-sin(gama).*sin(psiv);cos(gama)]; % d(ev)/dt gama
evpsi=[-sin(psiv); cos(psiv); zeros(size(gama))];              % d(ev)/dt psiv
```

```
function [Cd,Cl]=symNACA0015coef(ang,dor);
% function [Cd,Cl]=symNACA0015coef(ang,dor);
% dor: 1-units degree, 0-units radiu (default).
%  Chenwu Fan,  NOAP,  NPS
if(~exist('dor') | ~dor), ang=ang*180/pi; end
agcl=[0,0;1,0.045;2.5,0.23;4.7,0.5;6,0.7;9,0.9;10.05,0.95;12.5,1.055;14,0.95;15,0.62;
   16,0.6;17,0.59;18,0.585;20,0.6;22,0.61;25,0.68;30,0.88;35,0.99;40,1.02;45,1.03;
   50,1;55,0.94;60,0.86;65,0.75;70,0.6;75,0.47;80,0.35;85,0.21;90,0.09;93,0;
   100,-0.18;105,-0.3;110,-0.42;115,-0.58;120,-0.7;125,-0.785;130,-0.88;135,-0.98;
   140,-0.98;145,-0.9;150,-0.78;152.5,-0.7;155,-0.66;160,-0.62;165,-0.695;170,-0.89;
   175,-0.67;180,0];
agcd=[0,0;10,0.01;15,0.08;20,0.25;25,0.4;30,0.59;35,0.71;40,0.9;45,1.1;50,1.24;
   55,1.4;60,1.5;65,1.6;70,1.67;75,1.72; 80,1.76;85,1.8;90,1.81;95,1.78;100,1.73;
   105,1.68; 110,1.62;115,1.55;120,1.5;125,1.4;130,1.27;135,1.1;140,0.95;145,0.76;
   150,0.6;155,0.4;160,0.31;165,0.22;170,0.12;175,0.03;180,0.01];
Cd=interp1(agcd(:,1),agcd(:,2),ang);
Cl=interp1(agcl(:,1),agcl(:,2),ang);
```

```
function F3d = onefoilforce(vf3d,ee);
% function F3d = onefoilforce(vf3d,ee);
%  vf3d:  fin center velocity (3D)
%  ee:    bomb direction (unit vector)
%  F3d:   3-D force on one fin
%   C. Fan,  NOAP   NPS    9/21/2009
rw=1000; finarea=0.68^2;
vs=sqrt(sum(vf3d.^2));
if(vs<eps)
   F3d=zeros(3,1);
   return;
```

```
end
ev=vf3d/vs;
alpha=acos(sum(ev.*ee));
ealpha=cross(ev,ee);
ealpha=ealpha./(sqrt(sum(ealpha.^2))+eps);         % torque direction
el=cross(ealpha,ev);                                % lift direction
ed=-ev;                                             % drag direction
[Cd,Cl]=symNACA0015coef(alpha);
Fd=0.5*Cd*rw*finarea.*vs.^2;
Fl=0.5*Cl*rw*finarea.*vs.^2;
F3d=Fd*ed+Fl*el*0.6366;
```

```
function [OMG,IntOMG] = OMGsolve(lm,B,OMG0,dt);
% function [OMG,IntOMG] = OMGsolve(lm,BB,OMG0,dt);
%   Solve diagonal ODE as dOMG/dt = lm*OMG+ B, with the initial
%   condition OMG0 at time step dt.
%
%  Chenwu Fan,  NOAP,  NPS    4/10/2007
  if(lm<-1e-8)
    terminal=-B/lm; c=OMG0-terminal;
    OMG=c*exp(lm*dt)+terminal;
    IntOMG=terminal*dt+c/lm*(exp(lm*dt)-1);
  else
    OMG=OMG0+(B+lm*OMG0)*dt;
    IntOMG=OMG0*dt+(B+lm*OMG0)*dt^2/2;
  end
end
```

```
function Cm = MK84cm(elag,Re,del);
%  Chenwu Fan,  NOAP,  NPS
refRe=1.8e7;    % Critical Reynolds Number
re=Re/refRe;
Cm=NaN*zeros(size(re));
```

```
i1=find(elag<=pi/2);
Cm(i1)=0.07*sin(2*elag(i1))./re(i1).^0.2;
i2=find(elag>pi/2);
Cm(i2)=0.02*sin(2*elag(i2)).*re(i2).^0.5;
```

```
function cl=MK84cl(elag,Re,del);
%  Chenwu Fan,  NOAP,  NPS
% elag=abs(elag);
refRe=1.8e7;    % Critical Reynolds Number
re=Re/refRe;
cl=NaN*ones(size(Re));
i1=find(elag<=pi/2);
af1=pi*(2*elag(i1)/pi).^1.8;
cl(i1)=0.35*sin(af1).*re(i1).^0.2;
i2=find(elag>pi/2);
af2=2*pi*(2*elag(i2)/pi-1).^0.7;
cl(i2)=0.1*sin(af2)-0.015*del(i2).*re(i2).^2.*sin(af2.^0.85);
```

```
function cd = MK84cd(elag,Re,del);
%  Chenwu Fan,  NOAP,  NPS
% according to the scale model experiment, Re > 3x10^5 for bomb velocities
% > 7.80288 m/sec and drag coefficient < 0.2
refRe=1.8e7;    % Critical Reynolds Number
re=Re/refRe;
af=pi-2*elag;
% aff=sign(af).*sqrt(pi^2-(pi-abs(af)).^2);
% cd=0.02+0.25*exp(-(elag-pi/2).^2*2).*re.^0.2+0.008*sin(aff).*del;
N=2.2;
aff=sign(af).*(pi^N-(pi-abs(af)).^N).^(1/N);
cd=0.02+0.35*exp(-(elag-pi/2).^2*2).*re.^0.2+0.008*sin(aff).*del;
function [voli,areai,vcxi,Jx,Jy,cmd,cvd,xi,ri,xoi,cmr]=getbombphysics(xi,ri,CGx,m,denrat);
% function [voli,areai,vcxi,Jx,Jy,cmd,cvd,xi,ri,xoi,cfr,cmr]=getbombphysics(xi,ri,CGx,m,denrat);
% is used to calculate bomb physics parameters.
```

```
% input:
%    xi,ri:  the Bomb Radius data set (xi: distance from head)
%    CGx: center of Gravity (or mass) from front point (m)
%    m:  mass of bomb (kg)
%    denrat:  density ratio distribution as:[x,x2,x3,...;fac,fac2,fac3,...], default: [0,L;1,1]
% output:
%    voli:   volume data set
%    area:   conjection area data set
%    vcxi:   volume center data set (distance from head)
%    Jx,Jy:  Inertia around x, y axis
%    cmd:    center of mass distance, from volume center to mass center
%            (>0 Mc ahead of volume center)
%    cvd:    from volume to middle point. (>0 middle ahead of Vc)
%    xi,ri:  similar as input but add mass center point
%    xoi:    x variable based on mass center and head forward
%    cmr:    the anti-rotation torque coefficient Mr = -0.5*mw*C*|omg|*omg*L^2*cmr
%  Chenwu Fan,  NOAP,  NPS
if(~exist('denrat')), denrat=[0,xi(end);1,1]; end   % if the density ratio not input, then given a value of 1
if(size(xi,1)>1), xi=xi'; ri=ri'; end               % if bomb has a length then change row vector into column vector
ii1=find(xi<=CGx); ii2=find(xi>=CGx);               % finds and names the length that's less than or equal to and greater than or equal to
the center of gravity
if(ii1(end)~=ii2(1))                                % if they are not equal, then the radius must be found at the center of gravity
   ro=interp1(xi,ri,CGx);                           % the radius is interpolated at the center of gravity
   ri=[ri(ii1),ro,ri(ii2)];                         % the interpolated radius is then added to the radius matrix
   xi=[xi(ii1),CGx,xi(ii2)];                        % as well, the center of gravity is added to the length matrix
end
dxi=diff(xi);                                       % finds the distance between each point of length matrix
areai=(ri(1:end-1)+ri(2:end)).*dxi;                 % begins finding the 2D area by integrating the radius across the length of the bomb
areai=[0,areai]; areai=cumsum(areai);               % adds a zero/start point to the matrix; gives the total area in slices from beginning to
end of bomb
r11=ri(1:end-1).^2; r12=ri(1:end-1).*ri(2:end); r22=ri(2:end).^2;   % radii squared
```

```
dri=diff(ri);                                % finds the distance between each radius
voli=pi*(r11+r12+r22)/3.*dxi;                % frustum volumes (cylindar volume = pi*r^2)
vci=(r11+2*r12+3*r22)./(4*(r11+r12+r22)).*dxi;      % volume center of each slice
vcxi=vci+xi(1:end-1);                        % volume center locations along the bomb
faci=interp1(denrat(1,:),denrat(2,:),vcxi);         % volume center locations with density ratio factored in

Vco=sum(voli.*vcxi)/sum(voli);               % volume center (from nose of bomb)
cmd=Vco-CGx; cvd=Vco-xi(end)/2;              % center of mass=volume center-center of gravity;from volume to middle point
xoi=CGx-xi;                                  %  coordinate system moved to center of gravity (x variable based on mass center and head
forward)
[mmm,io]=min(abs(xoi));                      % finds the [value,location] of the minimum in the coordinate system
idxf=[1:io-1]; idxb=[io:length(vci)];        % creates front and back shapes
volf=sum(voli(idxf)); volb=sum(voli(idxb));         % creates front and back volumes
volxf=sum(voli(idxf).*faci(idxf).*(vcxi(idxf)-CGx));% front volume center locations with density ratio factored in
volxb=sum(voli(idxb).*faci(idxb).*(vcxi(idxb)-CGx));% back volume center locations with density ratio factored in
rhof=m*volxb/(volf*volxb-volb*volxf);        % density of front
rhob=m*volxf/(volb*volxf-volxb*volf);        % density of back
rhoi=rhof*faci;                              % density of back with density ratio factored in
rhoi(idxb)=rhob*faci(idxb);
vcxi=cumsum(vcxi.*voli)./cumsum(voli); vcxi=[0,vcxi];% the average cumulative sum of volume center locations along the bomb
voli=[0,voli]; voli=cumsum(voli);            % the cumulative sum of frustum volumes along the bomb
Jxi=(r11.^2+r12.*r11+r11.*r22+r12.*r22+r22.^2).*dxi.*rhoi*pi/10; % polar moment of inertia in x of sub-frustum
Jx=sum(Jxi);                                 % x-total polar moment of inertia
drdx=dri./diff(xoi); x1=xoi(1:end-1); x2=xoi(2:end); ri1=ri(1:end-1);
ridr=ri1-drdx.*x1;
JJi=ridr.^4.*(x1-x2)/4+ridr.^3.*drdx.*(x1.^2-x2.^2)/2+ridr.^2.*(1/3+drdx.^2/2).*(x1.^3-x2.^3)+...
   ridr.*drdx.*(1/2+drdx.^2/4).*(x1.^4-x2.^4)+drdx.^2.*(1/5+drdx.^2/20).*(x1.^5-x2.^5);% polar moment of inertia in y of sub-
frustum
Jy=pi*sum(rhoi.*JJi);                        % y-total polar moment of inertia
%  The anti rotation torque caused by rotation as Mr = -0.5*mw*C*|omg|*omg*L^2*cmr
xm=(x1+x2)/2;
```

```
ii1=find(xm>0);
cmr1=ridr(ii1).*(x1(ii1).^4-x2(ii1).^4)/4+drdx(ii1).*(x1(ii1).^5-x2(ii1).^5)/5;
ii2=find(xm<0);
cmr2=ridr(ii2).*(x1(ii2).^4-x2(ii2).^4)/4+drdx(ii2).*(x1(ii2).^5-x2(ii2).^5)/5;
cmr=2*[cmr1,-cmr2]; cmr=cumsum(cmr);
cmr=[0,cmr]/(voli(end)*xi(end)^2);
```

```
function cd2 = CdR28(Re);
% function cd2 = CdR28(Re);
%  Impact 28 Cross direction drag coefficient.
%
%  C. Fan   NOAP   NPS  9/10/2003
if (Re>=350000)
  cd2 = 1/(641550 / Re + 1.5);
elseif Re>=150000
  cd2 = 1.875 - .0000045 * Re;
elseif Re>= 12000
  cd2 = 1.2;              % aspect ratio?
elseif Re>= 2000
  cd2 = .84 + .00003 * Re;
elseif Re >= 180
  cd2 = .86 + 89 / Re;      % .855 +89/Re
elseif Re >= 12
  cd2 = 1.26 + 16 / Re;
elseif(Re>1e-10)
  cd2 = 1.8 + 8 / Re;       % 1.9276 + 8/Re
else
  cd2=0;
end
```

```
function [VS,GAMA,BETA,XYZ,OMG3D,psiv,psib]=bomb1step3D(dt,vs,gama,beta,xyz,omg3D,psiv,psib);
%   beta(el): bomb position elevation angle.
```

```
%   gama(ag): bomb velocity elevation angle.
%   psiv: bomb velocity azimuth angle
%   psib: bomb position azimuth angle
%   omg3D(del): bomb rotation velocity
%  Chenwu Fan,  NOAP,  NPS
global g rw m mw mwfl J L Lc d nu area yi areai voli vcyi cmr CGy yyy ...
      Re0 nfin
fff=1.85;
if(nfin==0), fff=0.7; end
% get 3D unit vectors
[ee,ev,ealpha,el,ed,evgama,evpsi]=setunitvector(gama,beta,psiv,psib);
% calculate attached angle
alpha=acos(sum(ev.*ee));
Re=vs*d/nu;   % initial reynolds number = initial velocity/(diameter of cylinder of equal volume*dynamic viscocity)
Lw=-xyz(3)+L/2; Lw=min(Lw,L); Lw=max(0,Lw);  % Under water bomb length
omg=sum(omg3D.*ealpha);    % angle velocity attached angle component
% calculate hydro dynamic coefficients: only drag coefficient effected by
% impact factor
Acd=MK84cd(alpha,Re,omg);
Acl=MK84cl(alpha,Re,omg);
Acm=MK84cm(alpha,Re,omg);
factimp=min(3,L/(Lw+eps)); % impact factor
Acd=Acd*factimp;
% As hydro force only effect the underwater part, must calculate the
% underwater project area(areaa), volume(voll), volume center(vcyy), and
% mass center (cmrr).
areaa=interp1(yi,areai,Lw);
voll=interp1(yi,voli,Lw);
vcyy=interp1(yi,vcyi,Lw);
cmrr=interp1(yi,cmr,Lw);
Fbuo=voll*rw*[0;0;g];    % 3D buoyancy force
```

```
rav2=rw*area*vs^2;
Fd=0.5*Acd*rav2; Fl=0.5*Acl*rav2;
F3dd=Fd*ed+Fl*el;        % 3D hydro dynamic force
F3d=F3dd+m*[0;0;-g]+Fbuo;  % total 3D force (hydro, gravity and buo forces)
Mt3d=0.5*Acm*rav2*L*ealpha;  % Hydro dynamic torque
Mf3d=cross((CGy-vcyy)*ee,F3dd);  % 3D hydro dynamic force torque
M3d=Mt3d+Mf3d;
if(nfin>0)
   if(xyz(3)<Lc-L)
      Mfbuo=cross(yyy*ee,mwfl*[0;0;g]);  % fin buoyancy torque
      Fbuo=Fbuo+mwfl*[0;0;g];   % add fin buoyancy
      F3d=F3d+mwfl*[0;0;g];   % add fin buoyancy
      Ff3D=onefoilforce(vs*ev+cross(omg3D,yyy*ee),ee)*nfin;
      F3d=F3d+Ff3D;   % add fin 3D forces
      Mf3df=cross(yyy*ee,Ff3D);
      M3d=M3d+(Mf3df+Mfbuo);  % add fin 3D torque
   end
end
M3d=M3d+cross((CGy-vcyy)*ee,Fbuo);   % add torque caused by Buoy
% As 3-D, M3d need seperate into OMG and (OMG x ee) direction componemts.
OMG=sqrt(sum(omg3D.^2));
if(OMG<1e-20), eomg=[1;0;0]; else, eomg=omg3D/OMG; end  % direction of OMG
eomgME=cross(eomg,ee);
eomgME=eomgME/sqrt(sum(eomgME.^2));   % direction of OMG x ee
Vax=sum(ev.*ee)*vs;
Vr3D=vs*ev-Vax*ee;
Vr=sqrt(sum(Vr3D.^2));
MrJ=-CdR28(Vr*d/nu)*rw*d*L^3*Vr/12/J/fff;  % anti rotation
% Calculate angle increase in OMG direction
MJ=sum(M3d.*eomg)/J;
[OMG,IntOMG] = OMGsolve(MrJ,MJ,OMG,dt);
```

```
IntOMG3D=IntOMG*eomg; OMG3D=OMG*eomg;
% calculate angle increase in normal OMG direction (OMG x ee)
MMEJ=sum(M3d.*eomgME)/J; incangME3D=0.5*MMEJ*dt^2*eomgME;
totlincang3D=IntOMG3D+incangME3D;
ebeta=[sin(psib);cos(psib);0];
dbeta=sum(totlincang3D.*ebeta);
BETA=beta+dbeta; psib=psib+totlincang3D(3);
As=sum(F3d.*ev)/m;     % speed accelerate
Dgama=sum(F3d.*evgama)/(m*vs);   % d(gama)/dt
Dpsiv=sum(F3d.*evpsi)/(m*vs);    % d(psi)/dt
agg=gama+Dgama*dt/2;     % middle step gama
psivm=psiv+Dpsiv*dt/2;  % middle step psiv
evm=[cos(agg).*cos(psivm); cos(agg).*sin(psivm); sin(agg)];% middle step ev
% update XYZ, gama & psiv
XYZ=xyz+(vs+As*dt/2)*dt*evm;
VS=vs+As*dt; GAMA=gama+Dgama*dt;
psiv=psiv+Dpsiv*dt;
% limit BETA & GAMA value with in (-pi,pi]
while(BETA>pi), BETA=BETA-2*pi; end
while(BETA<=-pi), BETA=BETA+2*pi; end
while(GAMA>pi), GAMA=GAMA-2*pi; end
while(GAMA<=-pi), GAMA=GAMA+2*pi; end
% update BETA and GAMA value within [-pi/2,pi/2]
if(BETA>pi/2), BETA=pi-BETA; psib=psib+pi; end
if(BETA<-pi/2), BETA=-pi-BETA; psib=psib+pi; end
while(psib>pi), psib=psib-2*pi; end
while(psib<=-pi), psib=psib+2*pi; end
if(GAMA>pi/2), GAMA=pi-GAMA; psiv=psiv+pi; end
if(GAMA<-pi/2), GAMA=-pi-GAMA; psiv=psiv+pi; end
while(psiv>pi), psiv=psiv-2*pi; end
while(psiv<=-pi), psiv=psiv+2*pi; end
```

THIS PAGE INTENTIONALLY LEFT BLANK

INITIAL DISTRIBUTION LIST

1. Defense Technical Information Center
   Ft. Belvoir, Virginia

2. Dudley Knox Library
   Naval Postgraduate School
   Monterey, California

3. Rear Admiral David Titley, USN
   Commander, Naval Meteorology and Oceanography Command
   Stennis Space Center, Mississippi

4. Rear Admiral (Sel) Jonathan White, USN
   Chief of Staff
   Commander, Naval Meteorology and Oceanography Command
   Stennis Space Center, Mississippi

5. Professor Peter Chu
   Naval Postgraduate School
   Monterey, California

6. Ronald Betsch
   MIW Program Manager
   Naval Oceanographic Office
   Stennis Space Center, Mississippi

7. Professor Jeffery Paduan
   Naval Postgraduate School
   Monterey, California

8. Admiral Richard Williams, USN (Ret)
   Naval Postgraduate School
   Monterey, California

9. Admiral Winford Ellis, USN (Ret)
   Naval Postgraduate School
   Monterey, California

10. Mr. Edward Gough
    Technical Director
    Commander, Naval Meteorology and Oceanography Command
    Stennis Space Center, Mississippi

11. Mr. Tom Cuff
Technical Director, Naval Oceanographic Office
Stennis Space Center, Mississippi

12. CAPT Robert Kiser, USN
Commander Oceanographic Operations
Commander, Naval Meteorology and Oceanography Command
Stennis Space Center, Mississippi

13. CAPT Scott Steadley, USN
Deputy Oceanographer of the Navy
Washington D.C.

14. CAPT Brian Brown, USN
Commanding Officer
Naval Oceanographic Office
Stennis Space Center, Mississippi

15. CAPT Paul Oosterling, USN
Commanding Officer
Naval Oceanographic Mine Warfare Center
Stennis Space Center, Mississippi

16. Mrs. Lori Wagner
Naval Oceanographic Office
Stennis Space Center, Mississippi

17. Mr. Brian Almquist
Ocean Engineering & Marine Systems
Office of Naval Research
Arlington, Virginia

18. Mr. Kennard Watson
Naval Surface Warfare Center, Panama City Division
Panama City, Florida

19. LCDR J. M. Bushnell, USN
Naval Postgraduate School
Monterey, California